AN INVESTIGATION OF THE DAMPING IN PITCH CHARACTERISTICS OF A TEN DEGREE CONE

A. M. Morrison, et al

Naval Surface Weapons Center
Silver Spring, Maryland

June 1975

NSWC/WOL/TR 75-84

NSWC

TECHNICAL REPORT

WHITE OAK LABORATORY

AN INVESTIGATION OF THE DAMPING IN PITCH CHARACTERISTICS OF A TEN DEGREE CONE

JUNE 1975

NAVAL SURFACE WEAPONS CENTER
WHITE OAK LABORATORY
SILVER SPRING, MARYLAND 20910

- Approved for public release; distribution unlimited

NAVAL SURFACE WEAPONS CENTER
WHITE OAK, SILVER SPRING, MARYLAND 20910

UNCLASSIFIED
SECURITY CLASSIFICATION OF THIS PAGE (When Data Entered)

REPORT DOCUMENTATION PAGE		READ INSTRUCTIONS BEFORE COMPLETING FORM
1. REPORT NUMBER NSWC/WOL/TR 75-84	2. GOVT ACCESSION NO.	3. RECIPIENT'S CATALOG NUMBER
4. TITLE (and Subtitle) An Investigation of the Damping in Pitch Characteristics of a Ten Degree Cone		5. TYPE OF REPORT & PERIOD COVERED 6. PERFORMING ORG. REPORT NUMBER
7. AUTHOR(s) A. M. Morrison J. E. Holmes W. R. Lawrence		8. CONTRACT OR GRANT NUMBER(s)
9. PERFORMING ORGANIZATION NAME AND ADDRESS Naval Surface Weapons Center White Oak Laboratory White Oak, Silver Spring, Maryland 20910		10. PROGRAM ELEMENT, PROJECT, TASK AREA & WORK UNIT NUMBERS
11. CONTROLLING OFFICE NAME AND ADDRESS		12. REPORT DATE June 1975 13. NUMBER OF PAGES 87
14. MONITORING AGENCY NAME & ADDRESS (if different from Controlling Office)		15. SECURITY CLASS. (of this report) Unclassified 15a. DECLASSIFICATION/DOWNGRADING SCHEDULE

16. DISTRIBUTION STATEMENT (of this Report)

Approved for public release; distribution unlimited.

17. DISTRIBUTION STATEMENT (of the abstract entered in Block 20, if different from Report)

18. SUPPLEMENTARY NOTES

19. KEY WORDS (Continue on reverse side if necessary and identify by block number)

Cone	Mach Number
Bluntness	Reynolds Number
Angle-of-Attack	Dynamic Stability

20. ABSTRACT (Continue on reverse side if necessary and identify by block number)

A series of one-degree-of-freedom dynamic wind tunnel measurements were made for a standard Supersonic Tunnel Association ten degree cone with varying bluntnesses of .25, .1, .0167, and .07. Variations of the stability coefficients with angle-of-attack, bluntness, Reynolds number, and Mach number are obtained including Mach 18 data points for which no previous data existed. An explanation of reported difference between

DD FORM 1 JAN 73 1473 EDITION OF 1 NOV 65 IS OBSOLETE
S/N 0102-014-6601

UNCLASSIFIED
SECURITY CLASSIFICATION OF THIS PAGE (When Data Entered)

measured dynamic stability as obtained from ballistic range and wind tunnel techniques is offered. The equations of motion, data reduction techniques and experimental methods are also developed.

NSWC/WOL/TR 75-84 27 June 1975

AN INVESTIGATION OF THE DAMPING IN PITCH CHARACTERISTICS OF A TEN DEGREE CONE

This report contains the results of an investigation of the dynamic stability characteristics of a ten degree cone at Mach numbers of 5 and 18. The equations of motion, data reduction method, and the experimental techniques are reviewed in detail in order to provide documentation for the dynamic testing techniques used at the Naval Surface Weapons Center. This work was sponsored by the Naval Sea Systems Command under the Aeroballistic Re-Entry Technology Program, L. Pasiuk, SEA-035, manager.

Acknowledgements are due Mr. Frank Regan and Mr. Sam Hastings of the Naval Surface Weapons Center, White Oak Laboratory, for their extensive assistance. Their help was and is greatly appreciated.

KURT R. ENKENHUS
By direction

CONTENTS

FIGURES

SYMBOLS

C_D	drag coefficient, D/QS
C_m	pitching-moment coefficient
C_{m_q}	damping-in-pitch derivative, $\partial C_m / \partial(qd/2V)$
C_{m_α}	static pitching-moment slope
d	reference length, maximum diameter
d_c	cone base diameter
D	drag force
I	transverse moment of inertia
K_j	initial modal amplitude, rad. or deg.
M	pitching moment
m	mass of missile, slugs
M_α	dimensional static pitch moment derivative, $\partial M / \partial \alpha$
$M_{\dot{\alpha}}$	dimensional damping pitch moment derivative, $\partial M / \partial \dot{\alpha}$
N	total pressure, atmospheres
P	pressure
P_c	surface pressure on cone
P_o	total pressure ahead of shock
Q	dynamic pressure, $1/2\rho V^2$
Q	quality factor of system
S	reference area, $\pi d^2/4$
s	Laplace transform variable
t	time

T	period of oscillation
V	free-stream airspeed
$\bar{V}$	airspeed ratio, model speed to free-stream airspeed
α	angle of attack
ζ	damping ratio
δ	logarithmic decrement
ψ	phase angle

Subscripts

o	total conditions, initial conditions
I	component of moment or displacement out of phase with applied moment
R	component of moment or displacement in phase with applied moment

INTRODUCTION

The Aeroballistic Re-entry Technology (ART) program of the Naval Surface Weapons Center has an objective to provide the aeroballistic technology required for the design and development of advanced re-entry body concepts. Essential to such an effort is the ability to predict, evaluate and modify aerodynamic characteristics of candidate configurations. Ground and flight test procedures, as well as computer modeling and analysis, are used in the general approach. Full-scale flight testing is complicated, costly and insecure, leaving ground testing as currently the most practical way to obtain aerodynamic data. The ballistic range and the hypervelocity wind tunnel are the most frequently used of the ground facilities in RV data gathering. Ballistic ranges have the obvious advantage of permitting measurements to be made in the absence of supports and their associated interference of the flow about the test body. However, range testing is costly on a per shot basis, flight parameters are difficult to control and data acquisition is very complicated. Nevertheless, it has been suggested that in wind-tunnel testing the flow interference due to supports results in uncertainties in the final results.[1] In order to determine if the Hypervelocity Facilities at NAVSURFWPNCEN are usable tools for studying re-entry body dynamic stability, a test program was undertaken.

The Supersonic Tunnel Association standard cone with varying nose bluntness was selected for testing. This configuration, a 10-degree half-angle cone, was chosen because it is representative of a classical re-entry shape and because extensive data exist for this configuration at lower Mach numbers. However, no dynamic data are available for this standard configuration at the operating Mach number (M = 18) of NAVSURFWPNCEN's Hypervelocity Research Tunnel.

Pitch damping measurements were made as a function of angle-of-attack, nose bluntness, Reynolds number and Mach number using the forced and free oscillation techniques. Data thus obtained are then compared with data from other facilities.

---

[1] Welsh, C. J., Winchenbach, G. L. and Madagan, A. N., "Free Flight Investigation of the Aerodynamic Characteristics of a Cone at High Mach Numbers," AIAA Journal, Vol. 8, No. 2, February 1970, pp. 294-300

While good agreement is noted with other wind tunnel data, there appears to be a significant discrepancy between these wind-tunnel measurements and the trend indicated by the range data. This paper will offer an explanation for this discrepancy based upon differences between in-plane and out-of-plane damping. Out-of-plane damping is present in the range tests but absent in the single-degree-of-freedom wind-tunnel measurements. The presentation format will include a derivation of the equation of motion of a one-degree-of-freedom system to include the effects of structural damping. In this section, the work on Orlik-Ruckemann,[2] Meirovitch,[3] and some nonreferencable analysis of F. J. Regan of the Naval Surface Weapons Center are heavily relied upon.

Next, the data reduction technique is discussed including a description of the Differential Correction Procedure and a listing of the Fortrav IV computer program utilized. Here the work of Eikenberry[4] and Nielsen[5] have contributed.

The one-degree-of-freedom free and forced oscillation systems are described and the wind tunnel tests conducted are outlined and results presented.

Finally, an explanation of the range and wind tunnel damping discrepancy is presented. This explanation is based on work recently completed at the Aerospace Research Laboratory.

---

[2]Orlik-Ruckemann, O., "Wind Tunnel Measurements of Dynamic Derivatives," Lecture Notes, University of Los Angeles, August 1963 (Available from National Research Council of Canada, Ottowa)

[3]Meirovitch, L., Analytical Methods in Vibrations, Macmillan Co., Callier-Macmillan Ltd., London, England, 1969

[4]Eikenberry, R. S., "Analysis of the Angular Motion of Missiles," SC-CR-70-6051, Sandia Laboratories, Albuquerque, New Mexico, February 1970

[5]Neilsen, K. L., Methods in Numerical Analysis, The Macmillan Co., New York, 1960

DEVELOPMENT OF THE EQUATIONS OF MOTION

The equation of motion of a viscously damped, one-degree-of-freedom oscillatory system can be expressed as:

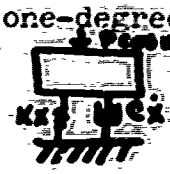

$$M\ddot{x} + C\dot{x} + Kx = P\cos\omega t \qquad (1)$$

for the forced oscillation case. If no external forcing functions are present, the system takes the form of a free oscillation represented by the homogenous equation:

$$M\ddot{x} + C\dot{x} + Kx = 0 \qquad (2)$$

In the above expression:

M is the mass	Mx is the inertial reaction
C is the damping coefficient	Cx is the damping reaction
K is the spring coefficient	Kx is the spring reaction
P is the forcing function amplitude	Pcoswt is the forcing function
x is the generalized coordinate	ω is the frequency of the forcing function

Consider a wind tunnel model at angle-of-attack (see Figure 1). If the model was not supported yet constrained to one-degree-of-freedome motion a pitching moment, due to the pressure induced normal force and a damping moment, always opposing oscillation would be generated. If the model were supported, such oscillations would occur about a trim angle-of-attack. This trim angle-of-attack is representative of a balance between the pitching moment and the moment generated by the support in response to its angular displacement (see Figure 2).

The instantaneous amplitude of the model about the trim angle, α_T, is represented by:

$$\bar{\alpha} = \alpha - \alpha_T \qquad (3)$$

For this trim angle case, equation (1) can be used to model the interaction of the moments acting.

$$I_y \frac{d^2\alpha}{dt^2} - \frac{QSd}{2V}\left[C_{mq}(\alpha)\right]\frac{d\alpha}{dt} - QSd\left[C_m(\alpha)\right] = M\sin\omega_f t + M_0 \qquad (4)$$

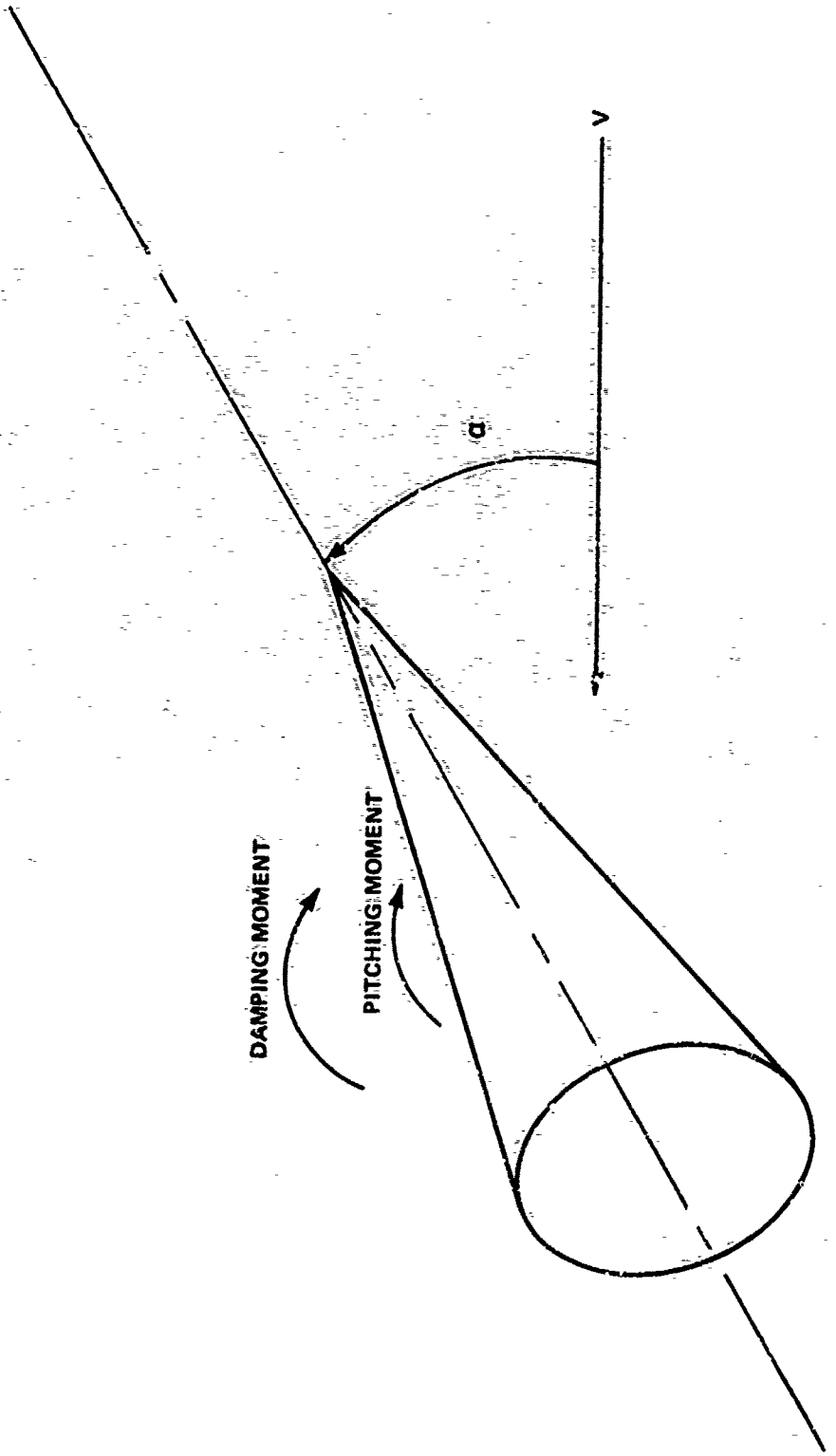

FIG. 1 MOMENTS ACTING ON WIND TUNNEL MODEL AT ANGLE-OF-ATTACK

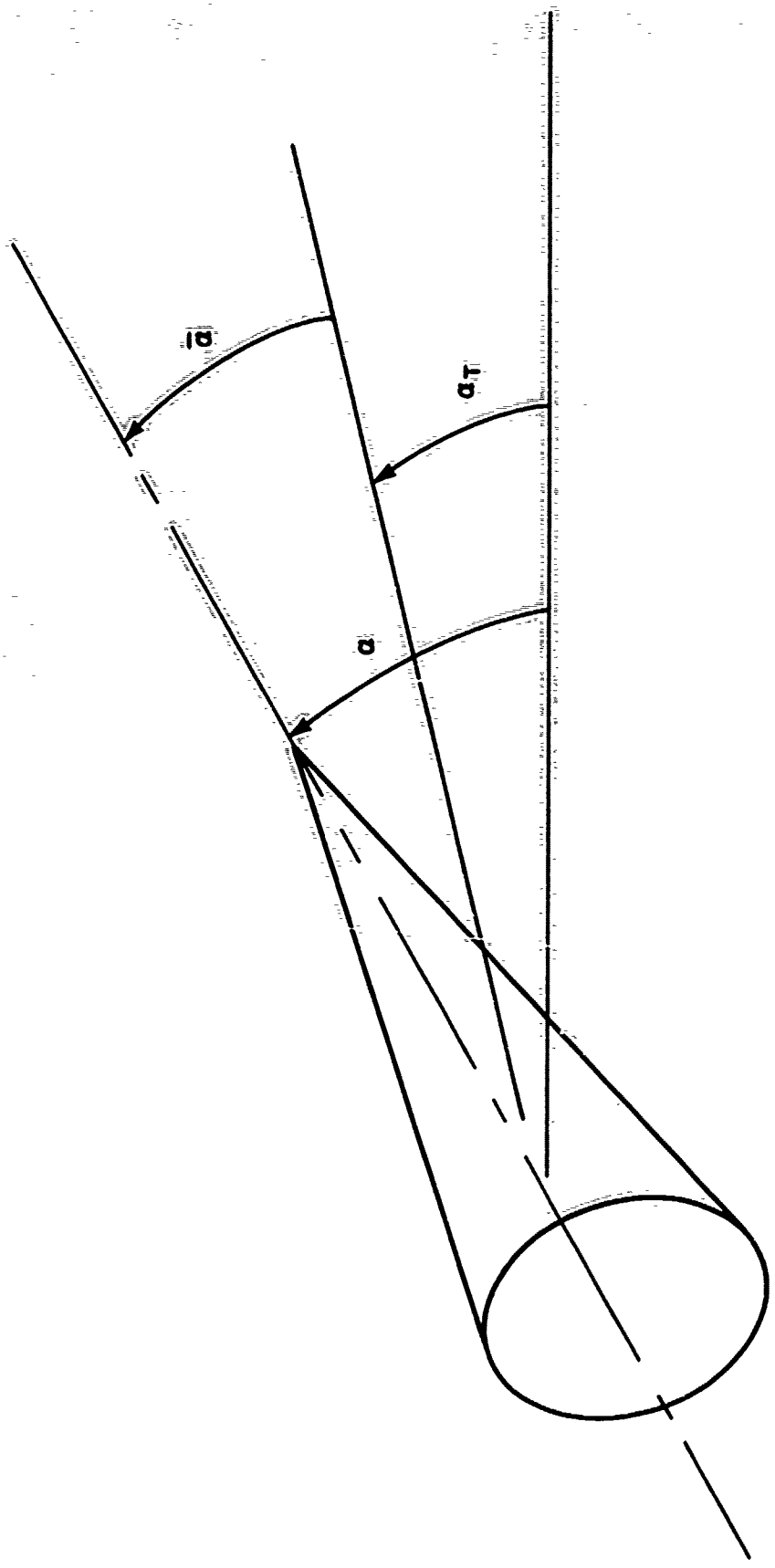

FIG. 2 ANGLE DEFINITION

Where I_y, Q, V, M and M_o are the moment of inertia, dynamic pressure, air speed, amplitude of time-dependent applied moment and trim moment required to maintain the trim angle. Consider the condition of $\alpha \ll 1$. Under this assumption, we can expand the damping derivative, C_{mq}, and the pitching moment term, C_m, in a series about the trim angle, α_T.

$$I_y \frac{d^2}{dt^2}[\bar{\alpha} - \alpha_T] - \frac{QSd}{2V}\left[C_{Mq}\Big|_{\alpha=\alpha_T}^{\bar{\alpha}} + \frac{dC_{Mq}}{d\alpha}\Big|_{\alpha=\alpha_T}^{\bar{\alpha}} + \frac{1}{2!}\frac{d^2C_{Mq}}{d\alpha^2}\Big|_{\alpha=\alpha_T}^{\bar{\alpha}^2} + \cdots\right]$$
$$\frac{d(\bar{\alpha}+\alpha_T)}{dt} - QSd\left[C_{M_o}\Big|_{\alpha=\alpha_T}^{\bar{\alpha}} + \frac{dC_M}{d\alpha}\Big|_{\alpha=\alpha_T}^{\bar{\alpha}} + \tfrac{1}{2!}\frac{d^2C_M}{d\alpha^2}\Big|_{\alpha=\alpha_T}^{\bar{\alpha}^2} + \cdots\right] \qquad (5)$$
$$= M \sin\omega_f t + M_o$$

Considering equation (4) for the case of steady state oscillation:

$$-QSd[C_M(\alpha)] = M_o$$

or

$$C_M(\alpha) = M_o/QSd \qquad (6)$$

which is representative of the pitch moment, support displacement generated moment previously mentioned. As the damping moment is an even function of α, its odd derivatives must vanish. The pitching moment is an odd function of α, thus its even derivatives must vanish. Including the above-mentioned considerations, equation (5) becomes:

$$I_y\frac{d^2\bar{\alpha}}{dt^2} - \frac{QSd^2}{2V}C_{Mq}\bar{\alpha}_T\frac{d\bar{\alpha}}{dt} - QSd\frac{dC_M}{d\alpha}\Big|_{\alpha=\bar{\alpha}_T} - \frac{QSd}{2V}\left[\tfrac{1}{2}\frac{d^2C_{Mq}}{d\alpha^2}\Big|_{\alpha=\bar{\alpha}_T}^{\bar{\alpha}^2} + \cdots\right]\frac{d\bar{\alpha}}{dt} - \left[\frac{QSd}{I}C_{M_\alpha}(\alpha_T)\right]\bar{\alpha} = \frac{M}{I}\sin\omega_f t \qquad (7)$$

If the angle of oscillation, $\bar{\alpha}$, is sufficiently small, equation (7) becomes:

$$\frac{d^2\bar{\alpha}}{dt^2} - \left[\frac{QSd^2}{2VI}C_{Mq}(\alpha_T)\right]\frac{d\bar{\alpha}}{dt} - \left[\frac{QSd}{I}C_{M_\alpha}(\alpha_T)\right]\bar{\alpha} = \frac{M}{I}\sin\omega_f t \qquad (8)$$

In order to be more concise, the equation (8) may be written in the form:

$$\frac{d^2\bar{\alpha}}{dt^2} - \left[\frac{QSd^2}{2VI}C_{Mq}\frac{d\bar{\alpha}}{dt}\right] - \left[\frac{QSd}{I}C_{M_\alpha}\right]\bar{\alpha} =$$
$$\ddot{\alpha} - \frac{M_{\dot{\alpha}}}{I}\dot{\bar{\alpha}} - \frac{M_\alpha}{I}\bar{\alpha} = P\sin\omega_f t \qquad (9)$$

The damping term, $M_{\dot{\alpha}}$, contains both aerodynamic and structural-mechanical damping and the stiffness term, M_{α}, contains both aerodynamic and mechanical stiffness.

The homogeneous form of equation (9) may be solved using the Laplace transform[6] as:

$$\mathcal{L}\{\ddot{\alpha}\} = \bar{\alpha}$$

with initial conditions:

$$\alpha|_{t=0} = \alpha_0$$
$$\dot{\alpha}|_{t=0} = \dot{\alpha}_0 = 0 \qquad (10)$$

Equation (9) then becomes:

$$s^2\bar{\alpha} - s\alpha_0 - s\left(\frac{M_{\dot{\alpha}}}{I}\right)\alpha_0 - \left(\frac{M_{\alpha}}{I}\right)\bar{\alpha} = 0 \qquad (11)$$

or rearranging yields:

$$\bar{\alpha} = \frac{\alpha_0\left(s - \frac{M_{\dot{\alpha}}}{I}\right)}{s^2 - \frac{M_{\dot{\alpha}}}{I}s - \frac{M_{\alpha}}{I}} \qquad (12)$$

Taking the inverse transform of equation (12) yields:

$$\alpha = \frac{\alpha_0}{\left[1 + \frac{(M_{\dot{\alpha}}/I)^2}{4(M_{\alpha}/I)}\right]} e^{\frac{M_{\dot{\alpha}}t}{2I}} \sin\left[\sqrt{\frac{-M_{\alpha}}{I}}\sqrt{1 + \frac{(M_{\dot{\alpha}}/I)^2}{4(M_{\alpha}/I)}}\, t + \psi\right] \qquad (13)$$

where

$$\psi = \tan^{-1}\left\{\frac{2\sqrt{\frac{M_{\alpha}}{I}}}{\frac{-M_{\dot{\alpha}}}{I}}\sqrt{1 + \frac{(M_{\dot{\alpha}}/I)^2}{4(M_{\alpha}/I)}}\right\} \qquad (14)$$

when $\left(\frac{M_{\dot{\alpha}}}{I}\right)^2 = -4\left(\frac{M_{\alpha}}{I}\right)$ the critically damped case occurs (all oscillatory motion ceases); when $M_{\dot{\alpha}} = 0$ the motion is undamped and the motion oscillates at a frequency of $\sqrt{M_{\alpha}/I}$. These two extremes of critically damped and undamped motion may be represented by the following parameters:

$$\zeta = \frac{-M_{\dot{\alpha}}/I}{2(-M_{\alpha}/I)^{1/2}} \qquad (15)$$

---

[6] Nixon, F. E., Handbook of Laplace Transforms, Prentice-Hall, Inc., Englewood Cliffs, New Jersey, 1960

The damping ratio represents the amount of damping present as a decimal fraction of the amount required for critical damping.

$$\omega_n = \sqrt{-M_\alpha / I} \tag{16}$$

is the undamped natural frequency.

Thus equations (13) and (14) may be rewritten:

$$\bar{\alpha} = \frac{\bar{\alpha}_0}{\sqrt{1-\zeta^2}} e^{-\zeta\omega_n t} \sin\left(\sqrt{1-\zeta^2}\, t + \psi\right) \tag{17}$$

$$\psi = \tan^{-1}\left\{\frac{\sqrt{1-\zeta^2}}{\zeta}\right\} \tag{18}$$

Equations (10) and (11) can also be used to rewrite equation (9) as:

$$\frac{d^2\bar{\alpha}}{dt^2} + 2\zeta\omega_n \frac{d\bar{\alpha}}{dt} + \omega_n^2 \bar{\alpha} = P_s \sin(\omega_f t) \tag{19}$$

Consider equation (17). The amplitude of the i th oscillation can be represented as:

$$\bar{\alpha}_i = \frac{\bar{\alpha}_0}{\sqrt{1-\zeta^2}} e^{-\zeta\omega_n t_i} \tag{20}$$

and the amplitude of the $(i+1)$th oscillation can be written as:

$$\bar{\alpha}_{i+1} = \frac{\bar{\alpha}_0}{\sqrt{1+\zeta^2}} e^{-\zeta\omega_n (t_i + T)} \tag{21}$$

where T is the period of oscillation.

The logarithm of the ratio of the succeeding amplitudes is:

$$\delta = \ln\left[\bar{\alpha}_i / \bar{\alpha}_{i+1}\right] = \ln\left[e^{\zeta\omega_n T}\right] = \zeta\omega_n T = \frac{2\pi\zeta\omega_n}{\omega_d} \tag{22}$$

where the damped frequency is ω_d. From equation (17) we obtain for the damped natural frequency, $\omega_d = \omega_n(\sqrt{1-\zeta^2})$. Thus the expression for the log-decrement, δ, becomes:

$$\delta = \frac{2\pi\zeta}{\sqrt{1-\zeta^2}} \approx 2\pi\zeta \qquad (\zeta \ll 1) \tag{23}$$

or

$$\zeta = \frac{\delta}{\sqrt{4\pi^2+\delta^2}} \approx \frac{\delta}{2\pi} \qquad (\delta \ll 1) \tag{24}$$

Thus the ratio of the logarithm of succeeding amplitudes, δ, may be related to the damping ratio, ζ. In a free-oscillation test the logarithm of the ratio of the initial amplitude, $\bar{\alpha}_0$, to the nth amplitude, $\bar{\alpha}_n$, follows from the definition of the log-decrement as:

$$n\delta = \ln(\bar{\alpha}_0/\bar{\alpha}_n) = 2\pi n\zeta \tag{25}$$

The number of oscillations required to damp to half amplitude for a model having a log-decrement, δ, and a damping ratio, ζ, is given as:

$$n_{1/2} = \frac{.694}{\delta} = \frac{.11}{\zeta} \tag{26}$$

and the number of cycles to damp to $1/e$ times the initial amplitude, $n_{1/e}$, is:

$$n_{1/e} = 1/\delta = \frac{.159}{\zeta} \tag{27}$$

other expressions of value are the time to damp to half amplitude, $\tau_{1/2}$, and the time to damp to $1/e$ of the initial amplitude or relaxation time, $\tau_{1/e}$, i.e., the time to damp to $1/e$ times the initial amplitude.

$$\tau_{1/2} = \frac{\ln 2}{\zeta\omega_n} \tag{28}$$

$$\tau_{1/e} = \frac{1}{\zeta\omega_n} \tag{29}$$

The equation of motion for a small amplitude free-oscillation system is given by equation (9) when the forcing function vanishes.

$$\frac{d^2\bar{\alpha}}{dt^2} - \frac{\hat{M}_{\dot{\alpha}}}{I}\frac{d\bar{\alpha}}{dt} - \frac{\hat{M}_{\alpha}}{I}\bar{\alpha} = 0 \tag{30}$$

In the free oscillation technique the model is mounted on a flexure, therefore account must be taken of the elastic stiffness in the $\hat{M}_{\alpha}$ term and the flexural damping in the $\hat{M}_{\dot{\alpha}}$ term.

In order to understand the flexural dampint contribution, an explanation of the concept of structural damping[3] is in order. The equation of motion could be rewritten in the generalized form as:

$$\ddot{X}(t) + 2\zeta\omega_n \dot{X}(t) + \omega_n^2 X(t) = \omega_n^2 f(t) = \omega_n^2 A e^{i\omega t} \tag{31}$$

The steady state response of the system to the harmonic excitation is given by the real part of:

$$X(t) = \frac{Ae^{i\omega t}}{1-(\omega/\omega_n)^2 + i2\zeta\omega/\omega_n} = H(w)\, Ae^{i\omega t} \tag{32}$$

where H(w) is the complex frequency response. We can write, however,

$$1 - \left(\frac{\omega}{\omega_n}\right)^2 + i2\zeta\frac{\omega}{\omega_n} = \left\{\left[1-\left(\frac{\omega}{\omega_n}\right)^2\right]^2 + \left(2\zeta\frac{\omega}{\omega_n}\right)^2\right\}^{1/2} e^{i\phi} \tag{33}$$

where the phase angle ϕ is,

$$\phi = \pm \tan^{-1} \frac{2\zeta\,\omega/\omega_n}{1-(\omega/\omega_n)^2} \tag{34}$$

Equation (32) can therefore be rewritten as:

$$X(t) = A|H(\omega)|\, e^{i(\omega t - \phi)} \tag{35}$$

which indicates that the complex vector describing the response x(t) lags behind the complex vector describing the excitation f(t) by the phase angle ϕ.

$$\dot{X}(t) = i\omega A|H(\omega)|e^{i(\omega t-\phi)} = i\omega X(t) \tag{36}$$

$$i = \cos \pi/2 + i \sin \pi/2 = e^{i\pi/2} \tag{37}$$

Equations (36) and (37) indicate that the velocity vector is 90° ahead of the displacement vector and ω times as large.

$$\ddot{X}(t) = (i\omega)^2 A|H(\omega)|\, e^{i(\omega t-\phi)} = -\omega^2 X(t) \tag{38}$$

The acceleration vector is 180° ahead of the displacement vector and ω^2 as large.

A complex vector plot relating the equations previously discussed is shown in Figure 3. All the vectors are harmonic functions of time with frequencies equal to the driving frequency ω. For steady state harmonic motion, the vectors rotate in the complex plane with frequency ω, while removing at the same relative position.

The energy dissipated by a viscously damped one-degree-of-freedom system per cycle of motion can be expressed as:

$$\Delta E_{CYCLE} = \int_0^{2\pi/\omega} F\,dx = \int_0^{2\pi/\omega} F\dot{x}\,dt \tag{39}$$

where only the real part of the impressed force F and the velocity $\dot{X}$ must be considered. Regarding A as a real number, which will not affect the result, yields:

$$\Delta E_{cycle} = M\omega_n^2 \int_0^{2\pi/\omega} Re[f(t)]\, Re[\dot{x}(t)]\,dt \tag{40}$$

$$= -M\omega_n^2 A^2 |H(\omega)|\,\omega \int_0^{2\pi/\omega} \cos\omega t \sin(\omega t-\phi)\,dt \tag{41}$$

$$= M\omega_n^2 A^2 |H(\omega)|\,\pi \sin\phi = C\pi\omega X^2 \tag{42}$$

where X is the maximum displacement amplitude and C is the damping coefficient.

With the above foundation in mind structural damping may now be considered. All real systems dissipate energy. The mass a spring system, previously illustrated, dissipate energy through internal friction. Unlike viscous damping, this type of damping does not depend on the time rate of strain. Kimball and Lovell[7] indicate that in a large variety of materials when subjected to cyclic stress, such that the stress remains below the ealstic limit, the internal friction is entirely

---

[7]Kimball, A. L. and Lovell, D. E., "Internal Friction in Solids," Phys. Rev., 30 (2nd Ser.), pp. 948-959, 1927

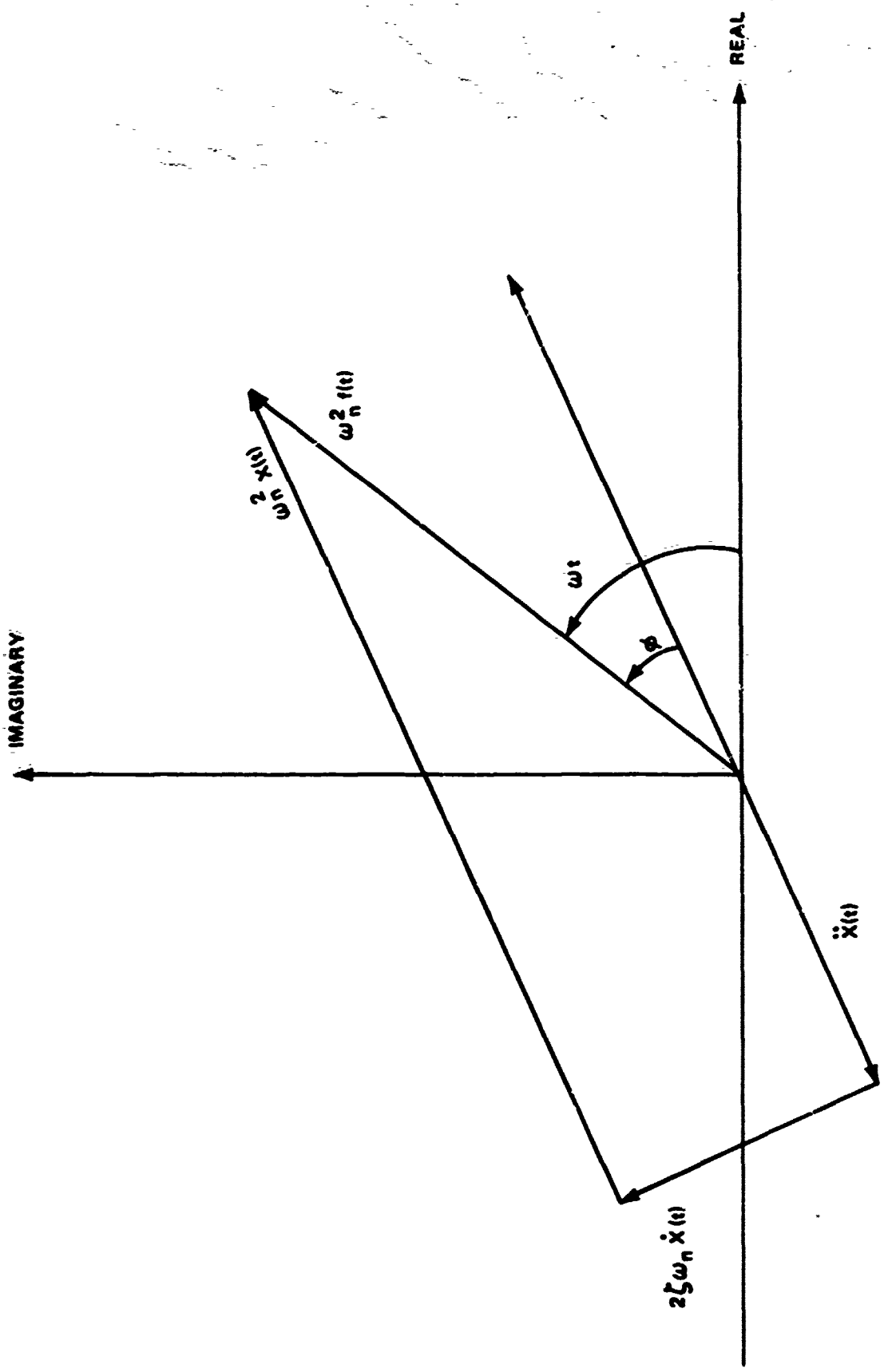

FIG. 3 VECTOR REPRESENTATION OF EQUATION (38)

independent of the rate of strain and depends on the amplitude of oscillation. The energy loss per cycle was found to be proportional to the amplitude squared

$$\Delta E_{CYCLE} = \alpha X^2 \tag{43}$$

where α is the constant of proportionality independent of the frequency of harmonic motion.

Similar behavior is exhibited by any elastic material. This type of damping is known as structural damping and is generally attributed to the hysterisis of the material or to friction between two components of the system. Even though this type of damping is independent of the frequency of the cycling stress, it is a phenomenon associated with cyclic stress as the energy dissipated in one cycle is proportional to the area within the hysterisis loop for the material (see Figure 4).

Therefore, one may treat a system subjected to harmonic excitation, with structural damping, as a viscously damped system with an equivalent viscous damping coefficient. Such a coefficient is suggested by comparing equations (42) and (43).

$$C_{eq.} = \frac{\alpha}{\pi \omega} \tag{44}$$

It is now possible to write the equation of motion of a one-degree-of-freedom system with harmonic excitation and structural damping as:

$$M\ddot{X}(t) + \frac{\alpha}{\pi\omega}\dot{X}(t) + KX(t) = KAe^{i\omega t} \tag{45}$$

Comparing the homogeneous forms of equations (19) and (45) suggests that:

$$\zeta \omega_n = \lambda = \frac{\alpha}{2\pi I \omega} \tag{46}$$

Account must be taken of the structural-mechanical and elastic stiffness as represented by terms with the "tilda" in equation (30). Again comparing equation (19) with $P=0$ and equation (30) yields:

$$2\zeta\omega_n = -\frac{\tilde{M}_{\dot{\alpha}}}{I} = -\left(\frac{M_{\dot{\alpha}}}{I} + \frac{\tilde{M}_{\dot{\alpha}}}{I}\right) \tag{47}$$

$$\omega_n^2 = -\frac{\tilde{M}_{\alpha}}{I} = -\left(\frac{M_{\alpha}}{I} + \frac{\tilde{M}_{\alpha}}{I}\right) \tag{48}$$

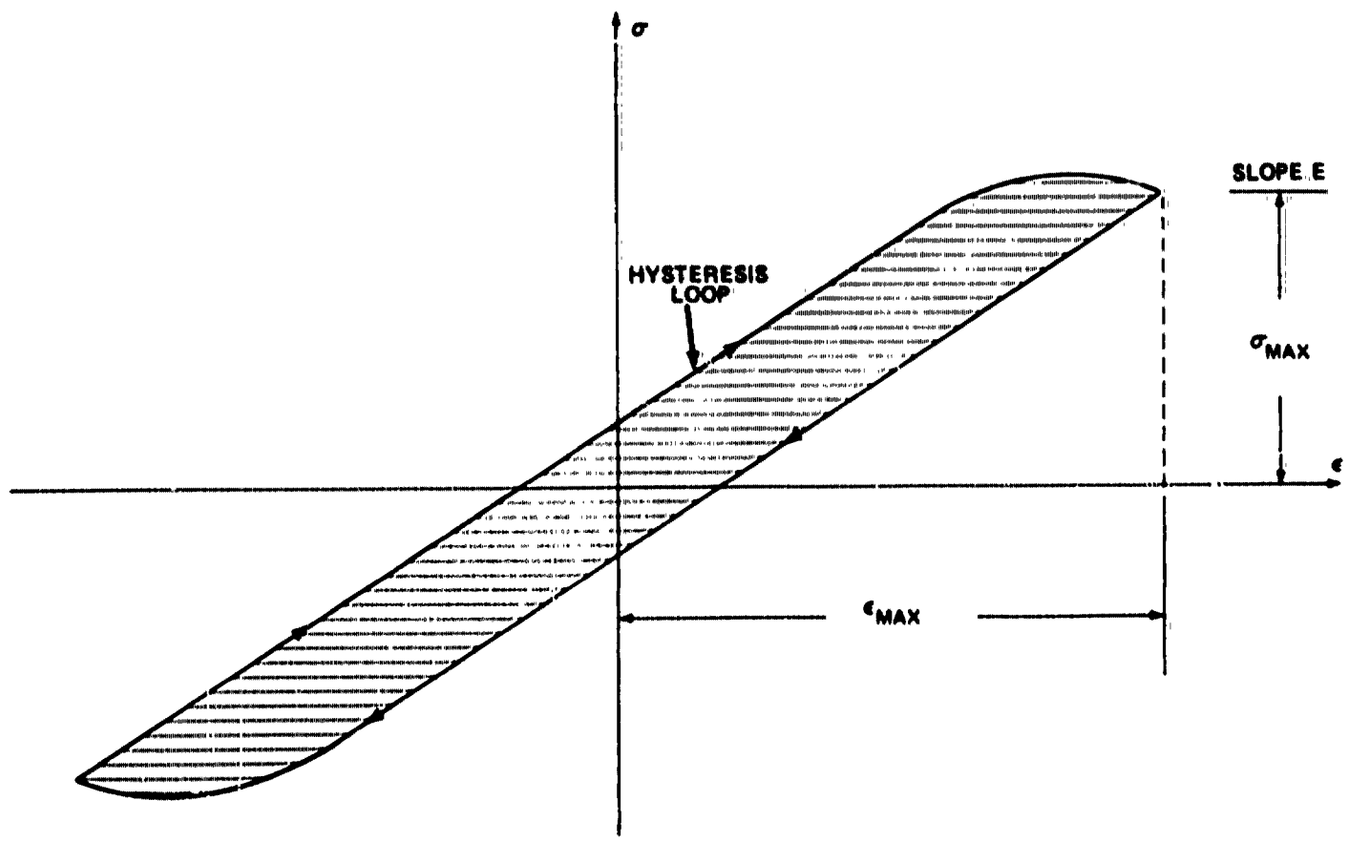

FIG. 4 HYSTERESIS LOOP, STRESS-STRAIN RELATION

The terms with the bar contain the mechanical-structural and stiffness contribution and the terms without the bars contain the aerodynamic contribution.

$$2\zeta_{\eta_0} = -\frac{\bar{M}_{\dot{\alpha}}}{I} = \frac{\alpha}{\pi I} \tag{49}$$

$$\omega_{\eta_0}^2 = -\frac{\bar{M}_{\alpha}}{I} = \frac{\omega_{d_0}^2}{1-\zeta_0^2} \tag{50}$$

Since we want the aerodynamic contributions alone we must evaluate the mechanical terms by permitting the model to oscillate in a vacuum or tare condition. Tare values are indicated by the subscript o. The total damping experienced may then be determined using equations (8), (46), and (47) as:

$$\frac{M_{\dot{\alpha}}}{I} = \left[\frac{\alpha}{\pi I \omega_d} + \frac{Qsd^2}{2VI} C_{mq}\right] \tag{51}$$

Some rearranging and combining with equation (46) yields:

$$\frac{\alpha}{\pi I \omega_d} = \frac{\alpha}{\pi I \omega_d}\left(\frac{\omega_{d_0}}{\omega_{d_0}}\right) = 2\lambda_0 \omega_{d_0}/\omega_d \tag{52}$$

which can be used to rewrite equation (51).

$$\frac{M_{\dot{\alpha}}}{I} = \left[2\lambda_0(\omega_{d_0}/\omega_d) + \frac{Qsd^2}{2VI} C_{mq}\right] = 2\lambda \tag{53}$$

Solving for C_{mq} yields:

$$C_{mq}\left[\frac{Qsd}{2VI}\right] = 2\lambda - 2\lambda_0 \omega_{d_0}/\omega_d \tag{54}$$

or,

$$C_{mq} = \frac{2VI}{Qsd}\left\{2\lambda - 2\lambda_0 \omega_{d_0}/\omega_d\right\} \tag{55}$$

where λ and ω_d refer to the values recorded with the wind tunnel on and λ_0 and ω_{d_0} refer to values obtained at the vacuum condition. The above could also be expressed in terms of the log decrement, δ, as:

$$C_{mq} = \frac{IV\omega_d}{Qsd^2}\left[\delta - \frac{\omega_{d_0}^2}{\omega_d^2}\delta_0\right] \tag{56}$$

The aerodynamic stiffness term may be found using essentially the same procedure,

$$M_\alpha = -I\left[\frac{\omega_d^2}{1-\zeta^2} - \frac{\omega_{d_0}^2}{1-\zeta_0^2}\right] \cong -I\left[\omega_d^2(1+\zeta^2) - \omega_{d_0}^2(1+\zeta_0^2)\right] \tag{57}$$

or making use of the log decrement, δ , as,

$$M_\alpha \cong -I\left[\omega_d^2\left(1+\frac{\delta^2}{4\pi^2}\right) - \omega_{d_0}^2\left(1+\frac{\delta_0^2}{4\pi^2}\right)\right] \tag{58}$$

and in coefficient form,

$$C_{M_\alpha} \cong -\frac{I}{qsd}\left[\omega_d^2(1+\zeta^2) - \omega_{d_0}^2(1+\zeta_0)\right] \tag{59}$$

or

$$C_{M_\alpha} \cong -\frac{I}{qsd}\left[\omega_d^2\left(1+\frac{\delta^2}{4\pi^2}\right) - \omega_{d_0}^2\left(1+\frac{\delta_0^2}{4\pi^2}\right)\right] \tag{60}$$

The equations of motion of a one-degree-of-freedom viscously damped (including structural damping) system system have been developed from the general case. Forms have been generated which allow calculation of the damping moment coefficient, the pitching moment coefficient based on trim angle, and the slope of the pitching moment coefficient. In order to evaluate these expressions parameters must be obtained for a wind tunnel on case and for a vacuum or tare case.

SMALL AMPLITUDE FORCED OSCILLATION

In the forced oscillation system a moment, $\bar{M} = M \sin\omega_f t$, is applied to the model. The desired measurement is primarily the damping-in-pitch derivative, C_{m_q}, and to a lesser extent the local tangent to the static pitching moment coefficient, $C_{m_\alpha}\big|_{\alpha=\alpha_T}$. It will now be shown that it is necessary to measure the magnitude of the applied moment, the angular displacement and the phase angle between these two quantities.

The equation of motion for the forced oscillation system is given in equation (9). A first integral of this equation may be obtained by integrating over one period as,

$$I\int_0^{2\pi}\ddot{\alpha}\,d\tau + \tilde{M}_{\dot{\alpha}}\int_0^{2\pi}\dot{\alpha}\,d\tau + \tilde{M}_\alpha\int_0^{2\pi}\alpha\,d\tau = M\int_0^{2\pi}\sin\omega_f t\,d\tau \tag{61}$$

or changing the variable of integration

$$I\int_0^{\tau}\ddot{\alpha}\,\dot{\alpha}\,dt + \tilde{M}_{\dot{\alpha}}\int_0^{\tau}\dot{\alpha}^2 dt + \tilde{M}_{\alpha}\int_0^{\tau}\dot{\alpha}\,\alpha\,dt = M\int_0^{\tau}\sin\omega_f t\,\dot{\alpha}\,dt \qquad (62)$$

The steady state solution of equation (9) is given by making use of Laplace transforms, equation (9) becomes:

$$s^2\bar{\alpha} - s\alpha_0 + 2\zeta\omega_n(s\bar{\alpha}-\alpha_0) + \omega_n^2\bar{\alpha} = \frac{P\omega_f}{s^2+\omega_f^2} \qquad (63)$$

$$\omega_n^2\bar{\alpha}\left[\frac{s^2}{\omega_n^2} + \frac{2\zeta}{\omega_n}s + 1\right] = 2\zeta\omega_n\alpha_0\left[\frac{s}{2\zeta\omega_n}+1\right] + \frac{P/M_f}{\left(\frac{s}{\omega_f}\right)^2+1} \qquad (64)$$

Now solving for $\bar{\alpha}$ we get:

$$\bar{\alpha} = \frac{\frac{2\zeta\alpha_0}{\omega_n}\left[\frac{s}{2\zeta\omega_n}+1\right]}{\left[\frac{s^2}{\omega_n^2}+\frac{2\zeta}{\omega_n}s+1\right]} + \frac{\frac{P\omega_f}{\omega_n^2\omega_f^2}}{\left[\frac{s^2}{\omega_n^2}+\frac{2\zeta s}{\omega_n}+1\right]\left[\left(\frac{s}{\omega_f}\right)^2+1\right]} \qquad (65)$$

Since the inverse transform operation, $\mathcal{L}^{-1}\{\}$, is linear, we can regard the inverse transforms separately: The first term on the right is the transient solution with the inverse of this term already obtained in equation (17). As has been pointed out, equation (18) represents the angular motion of the model during free oscillation. For the forced oscillation technique we can regard the system as starting from rest, i.e., $\alpha_0 = 0$, in which case the first term on the right of equation (65) vanishes. The inverse transform of the second term on the right of equation (65) is as follows:

$$\alpha(t) = \frac{P\omega_f}{\left[(\omega_n^2-\omega_f^2)^2+4\zeta^2\omega_n^2\omega_f^2\right]^{1/2}}\left[\tfrac{1}{2}\omega_f\sin(\omega_f t-\psi_1)\right] + \left[1/(\omega_n\sqrt{1-\zeta^2})\right]e^{-\zeta\omega_n t}\sin(\omega_f t-\psi_2) \qquad (66)$$

where

$$\psi_1 = \mathrm{Tan}^{-1}\left\{\frac{2\zeta\omega_f\omega_n}{\omega_n^2-\omega_f^2}\right\} \qquad (67)$$

and

$$\psi_2 = \mathrm{Tan}^{-1}\left\{\frac{-2\zeta\omega_n^2\sqrt{1-\zeta^2}}{\omega_f^2-\omega_n^2(1-2\zeta^2)}\right\} \qquad (68)$$

Even in equation (66) we have a transient solution in the second term which accounts for bringing the system from rest to the steady-state forcing frequency. This transient would be superimposed upon the transient represented by equation (17) if $\bar{\alpha}_o$ is not zero. Since we are interested in the steady-state conditions, only the first term on the right of equation (66) will be retained. This term may be rewritten in a slightly different, but more useful, form as,

$$\bar{\alpha}(t) = \frac{P/\omega_n^2}{\left[\left(1-\left(\frac{\omega_f}{\omega_n}\right)^2\right)^2+4\zeta^2\left(\frac{\omega_f}{\omega_n}\right)^2\right]} \sin(\omega_f t-\psi) \tag{69}$$

$$= K(\zeta, \omega_f/\omega_n) \sin(\omega_f t-\psi)$$

where

$$\psi = \text{TAN}^{-1}\left\{\frac{2\zeta\left(\frac{\omega_f}{\omega_n}\right)}{1-\left(\frac{\omega_f}{\omega_n}\right)^2}\right\} = \sin^{-1}\left\{\frac{2\zeta\left(\frac{\omega_f}{\omega_n}\right)}{\left[\left(1-\left(\frac{\omega_f}{\omega_n}\right)^2\right)^2+4\zeta^2\left(\frac{\omega_f}{\omega_n}\right)^2\right]^{1/2}}\right\} \tag{70}$$

Resonance occurs when the amplitude of the sine function of equation (69) attains a maximum value. In the absence of damping resonance occurs when

$$\frac{\omega_f}{\omega_n} = 1 \tag{71}$$

and in the presence of damping resonance occurs when

$$\frac{\omega_f}{\omega_n} = \sqrt{1-2\zeta^2} \tag{72}$$

Resonance is often said to occur when the forcing frequency, ω_f, equals the undamped natural frequency, ω_n. This statement is true only when the system has no damping, although it may be an acceptable approximation for low levels of damping.

The above expression is easily derived by taking the derivative of the amplitude in equation (69) with respect to $(\omega_f/\omega_n)^2$, equating this derivative to zero and solving to obtain equation (72). Inserting (72) into (69) gives the amplitude at resonance as

$$K(\zeta, \omega_f/\omega_n) = \frac{P/\omega_n^2}{2\zeta(1-\zeta^2)^{1/2}} = K_R \tag{73}$$

Also at resonance, the phase angle, ψ (eq. (70)) becomes,

$$\psi_R = \sin^{-1}\left(\frac{1-2\zeta^2}{1-\zeta^2}\right)^{1/2} \tag{74}$$

The angle, ψ, is known as the phase angle and it may be seen from equation (69) that the angular displacement lags the applied moment by the angle ψ. The applied moment from equation (4) is:

$$\bar{M}(t) = M \sin \omega_f t \tag{75}$$

and the angular displacement follows from equation (69) as,

$$\bar{\alpha}(t) = K\left(\zeta, \frac{\omega_f}{\omega_n}\right) \sin\left(\omega_f t - \psi\right) \tag{76}$$

The relative position of the moment and angular displacement functions, $\bar{M}(t)$ and $\bar{\alpha}(t)$, respectively, are given in Figure 5.

Since we are considering a lightly damped system (damping ratio less than 0.1) a first guess at the phase angle might be 90 degrees. However, the damping ratio, though small, is influential at resonance both in the angular displacement amplitude (viz., eq. (73)) and in setting the phase angle exactly. Clearly equation (74) may be rewritten as,

$$\sin\psi = \frac{1-2\zeta^2}{1-\zeta^2} = 1 - \frac{\zeta^2}{1-\zeta^2} \tag{77}$$

Since the actual phase angle will be slightly less than $\pi/2$, we may introduce a small positive quantity, ϵ, as

$$\psi = \pi/2 - \epsilon \tag{78}$$

Equation (77) becomes

$$\sin^2(\pi/2 - \epsilon) = \cos^2\epsilon = 1 - \frac{\zeta^2}{1-\zeta^2} \tag{79}$$

or

$$\sin\epsilon = \frac{\zeta}{(1-\zeta^2)^{1/2}}$$

or solving the above expression for the damping ratio, ζ, we get

$$\zeta = \frac{\sin\epsilon}{\left[1+\sin^2\epsilon\right]^{1/2}} \tag{80}$$

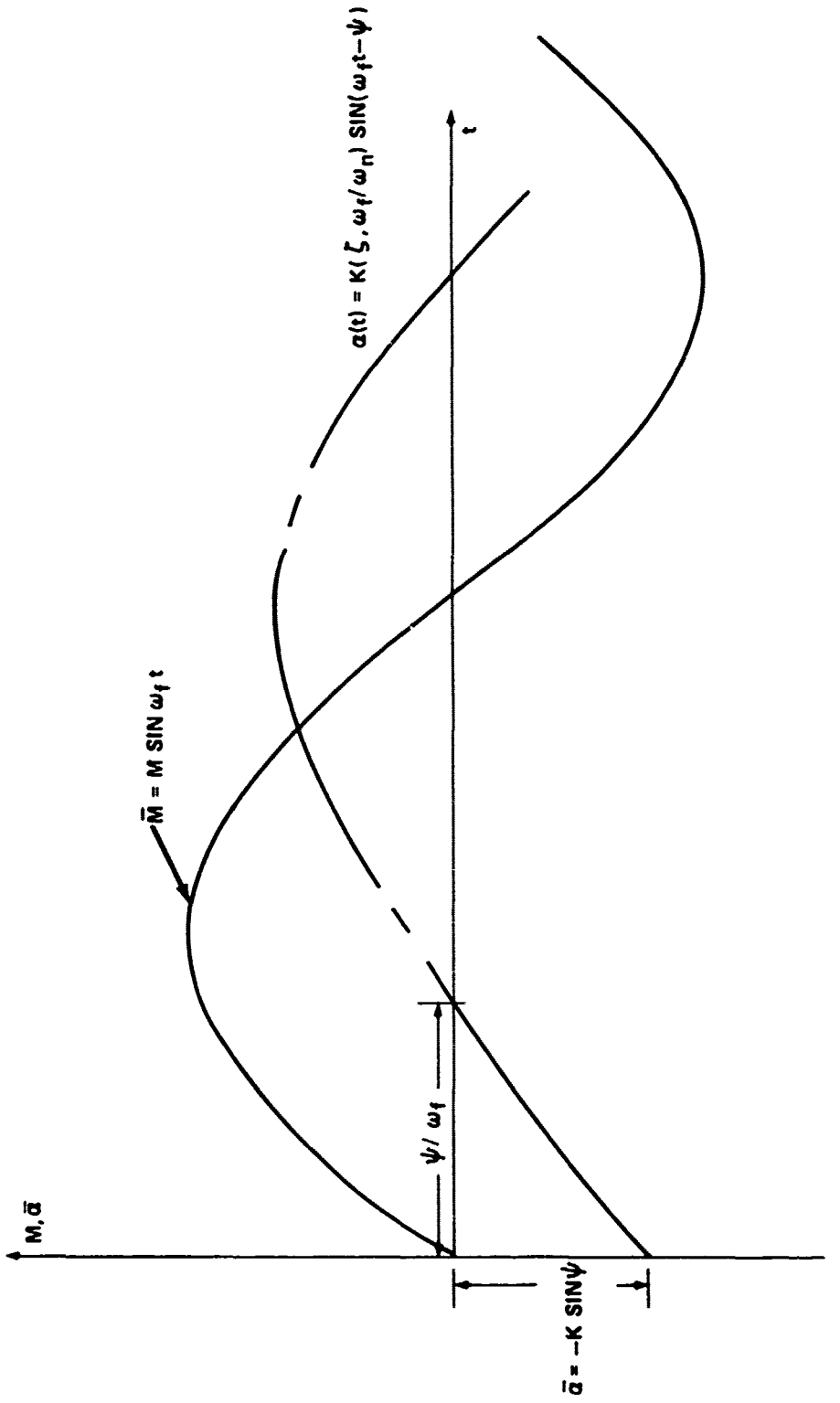

FIG. 5 MOMENT AND ANGULAR DISPLACEMENT VS TIME

Clearly, equation (79) allows the following approximation for small values of damping ratio,

$$\varepsilon \cong \zeta \tag{81}$$

Thus in order to measure the damping ratio (and hence the damping-in-pitch derivative from equation (15)) it is clear that the phase angle, ψ, or the term, ε, must be measured accurately. Equation (69) together with the first and second derivative may be written as,

$$\bar{\alpha} = K \sin(\omega_f t - \psi) \tag{82}$$

$$\dot{\bar{\alpha}} = \omega_f K \cos(\omega_f t - \psi) \tag{83}$$

$$\ddot{\bar{\alpha}} = -\omega_f^2 K \sin(\omega_f t - \psi) \tag{84}$$

Inserting the above expression into equation (62) where appropriate gives,

$$-I\omega_f^3 K^2 \int_0^\tau \cos(\omega_f t - \psi)\sin(\omega_f t - \psi)\,dt - \tilde{M}_{\dot{\alpha}} \omega_f^2 K^2 \int_0^\tau \cos^2(\omega_f t - \psi)\,dt$$
$$- \tilde{M}_{\alpha} \omega_f K^2 \int_0^\tau \sin(\omega_f t - \psi)\cos(\omega_f t - \psi)\,dt = MK\omega_f \tag{85}$$
$$\int_0^\tau \sin\omega_f t \cos(\omega_f t - \psi)\,dt$$

Clearly the first and third terms on the left are zero so we are left with,

$$-\tilde{M}_{\dot{\alpha}} \omega_f^2 K^2 \int_0^\tau \cos^2(\omega_f t - \psi)\,dt = MK\omega_f \int_0^\tau \sin\omega_f t \cos\omega_f t$$
$$\cos\psi\,dt + MK\omega_f \int_0^\tau \sin^2\omega_f t \sin\psi\,dt \tag{86}$$

The first term on the right is easily shown to be zero so equation (86) becomes,

$$-\tilde{M}_{\dot{\alpha}} \omega_f^2 K^2 \frac{\tau}{2} = MK\omega_f \sin\psi \frac{\tau}{2}$$

or

$$\tilde{M}_{\dot{\alpha}} = -\frac{M}{\omega_f K}\sin\psi \tag{87}$$

It was pointed out in the case of free oscillations (equations (30) and (31)) that structural damping must be removed. Thus, equation (87) becomes,

$$M_{\dot{\alpha}} = \tilde{M}_{\dot{\alpha}} - \bar{M}_{\dot{\alpha}}$$

or

$$M_{\dot{\alpha}} = -\left(\frac{M}{\omega_f K}\sin\psi - \frac{M_o \sin\psi_o}{\omega_{f_o} K_o}\right) \tag{88}$$

The above expression is considered to be the basic data-reduction equation for measuring the damping-in-pitch derivative using the forced oscillation technique. This equation appears as equation (6) in reference 6, as equation (42) in reference 2 and as equation (25) in reference 9.[8,9] Along the lines of equation (56), equation (88) might be written in coefficient form as

$$C_{M_q} + C_{M_{\dot{\alpha}}} = -\frac{2V}{qSd^2}\left[\frac{M\sin\psi}{\omega_f K} - \frac{M_o \sin\psi_o}{\omega_{f_o} K_o}\right] \tag{89}$$

It should be pointed out that for a finite amount of damping resonance is reached somewhat before ω_f/ω_n equals unity (see equation (72)) and at resonance the phase angle is less than 90 degrees (see equation (74)). From equations (72) and (74) we have for effects of the order ζ^2:

$$\omega_f/\omega_n = 1 - \zeta^2 \tag{90}$$

$$\sin\psi_R = 1 - \tfrac{1}{2}\zeta^2 \tag{91}$$

---

[8]Mackapetris, L. J., "A Forced Oscillation System for Measuring Damping Derivatives at Subsonic and Transonic Speeds," Naval Ship Research and Development Center Report 2627, November 1967

[9]Wiley, H. G., "A Method for Accurately Measuring Dynamic Stability Derivatives in Transonic and Supersonic Wind Tunnels," Presented to AGARD Specialists Meeting, Aircraft Stability and Control (Available from NASA, Langley Research Center), April 1961

Quite obviously for lightly damped systems (ζ about 0.1 or less) there is negligible error in oscillating the model at the undamped natural frequency.

Actually, the undamped natural frequency, ω_n, is a somewhat artificial quantity in that it is not directly measureable damped natural frequency, ω_d, and the damping ratio, ζ, which is expressible in terms of the log-decrement, δ (equations (22)-(29)). From equation (17):

$$\omega_d = \omega_n (1-\zeta^2)^{1/2} \tag{92}$$

From equation (72), the ratio of the forcing frequency, ω_f, to the undamped natural frequency, ω_n, under conditions of resonance is,

$$\left.\frac{\omega_f}{\omega_n}\right|_R = (1-2\zeta^2)^{1/2} \tag{93}$$

which gives,

$$\left.\frac{\omega_f}{\omega_d}\right|_R = \frac{(1-2\zeta^2)^{1/2}}{(1-\zeta^2)^{1/2}} \tag{94}$$

where the relationship with the phase angle follows from equation (74). Thus, at resonance the ratio of the driving frequency, ω_f, to the damped natural frequency, ω_d, is equal to $\sin\psi_R$.

While the primary goal of the small amplitude forced oscillation technique is to obtain the damping-in-pitch derivative, C_{m_q}, it is possible to also obtain the local tangent to the static pitching moment, i.e., C_{m_α}. From equation (69) we have,

$$K\left(\frac{\omega_f}{\omega_n},\zeta\right) = \frac{P/\omega_n^2}{\left[\left(1-\left(\frac{\omega_f}{\omega_n}\right)^2\right)^2+4\zeta^2\left(\frac{\omega_f}{\omega_n}\right)^2\right]^{1/2}} \tag{95}$$

and from equation (70)

$$\cos\psi = \frac{1-\left(\frac{\omega_f}{\omega_n}\right)^2}{\left[\left(1-\left(\frac{\omega_f}{\omega_n}\right)^2\right)^2+4\zeta^2\left(\frac{\omega_f}{\omega_n}\right)\right]^{1/2}} \tag{96}$$

Thus equation (95) may be rewritten as,

$$K\left(\frac{\omega_f}{\omega_n}, \zeta\right) = \frac{P\cos\psi}{\omega_n^2\left(1-\left(\frac{\omega_f}{\omega_n}\right)^2\right)} \tag{97}$$

Now from equation (48)

$$K\left(\frac{\omega_f}{\omega_n}, \zeta\right) = \frac{P\cos\psi}{\omega_n^2 - \omega_f^2} = \frac{P\cos\psi}{-\frac{M_\alpha}{I} - \frac{\bar{M}_{\dot\alpha}}{I} - \omega_f^2} \tag{98}$$

or

$$-\frac{M_\alpha}{I} - \frac{\bar{M}_{\dot\alpha}}{I} - \omega_f^2 = \frac{P\cos\psi}{K} \tag{99}$$

In a vacuum the structural damping contributions are alone present,

$$\bar{M}_{\dot\alpha} = -\frac{M_0\cos\psi_0}{K_0} - I\omega_{f_0}^2 \tag{100}$$

Using equation (100) in equation (99), the static moment derivative due to aerodynamic effects is

$$M_\alpha = -\left[\frac{M\cos\psi}{K} - \frac{M_0\cos\psi_0}{K}\right] - I(\omega_f^2 - \omega_{f_0}^2) \tag{101}$$

The assumption has been made that the mechanical damping is proportional to the oscillatory frequency. Vacuum conditions are designated by the subscript "o." Equation (101) may be rewritten in coefficient from as

$$C_{M_\alpha} = -\frac{1}{qsd}\left\{\left(\frac{M\cos\psi}{K} - \frac{M_0\cos\psi_0}{K_0}\right) - I(\omega_f^2 - \omega_{f_0}^2)\right\} \tag{102}$$

Equations (101) and (102) are the data-reduction equations for the determination of the static moment from the small amplitude forced oscillation technique. Equations (101) and (102) appear as equation (24) in reference 8, as equation (43) in reference 2, and equation (26) in reference 9.

Further simplifications are possible in equations (101) and (102). If the drive frequency is identical in both the wind-on and wind-off conditions then the second term in equations (101) and (102) vanishes to give,

$$C_{M_\alpha} = -\frac{1}{qsd}\left\{\frac{M\cos\psi}{K} - \frac{M_0\cos\psi_0}{K_0}\right\} \tag{103}$$

In driving at resonance the phase angle, $\psi = \psi_R$, is such that

$$\cos\psi_R = \frac{\zeta}{(1-\zeta^2)^{1/2}} \approx \zeta \tag{104}$$

a result that follows readily from equation (74). Clearly equation (104) shows that for the lightly damped system $\cos\psi_R$ will be very small and approximately equal to the damping ratio.

Another concept worth noting is the "Q" or quality factor of the system. The Q of the system is defined as the ratio of the amplitude under dynamic conditions to the amplitude under static conditions, i.e.,

$$Q = \frac{|\alpha(t)|}{\alpha_s} \tag{105}$$

The static deflection, α_s, may be obtained from equation (19) by setting $\ddot{\alpha} = \dot{\alpha} = 0$ to obtain,

$$\alpha_s = P/\omega_n^2 \tag{106}$$

The appearance of frequency, ω_n, in the evaluation of a static effect might be misleading. In equation (16) it is shown that the undamped natural frequency, ω_n, is determined by the static moment derivative, M_α. From equations (76) and (95) we get for Q,

$$Q = \frac{|\alpha(t)|}{\alpha_s} = \frac{1}{\left\{\left(1-\left(\frac{\omega_1}{\omega_n}\right)^2\right)^2 + 4\zeta^2\left(\frac{\omega_1}{\omega_n}\right)^2\right\}^{1/2}} \tag{107}$$

For oscillations at resonance we may find Q_R using equation (72) as

$$Q_R = \frac{1}{2\zeta(1-\zeta^2)} \approx \frac{1}{2\zeta} \tag{108}$$

or using equation (23)

$$Q_R \cong \frac{\pi}{\delta} \tag{109}$$

Equation (107) indicates that for a lightly damped system it is necessary to oscillate almost exactly at resonance to see any amplification of the static response. Equations (108) and (109) show that when resonance is closely approached there will be a sudden increase in the amplitude of the model. Equation (70) points out that for a lightly damped system, the phase angle will

be zero until very close to resonance at which point it will be near to $\pi/2$ (although as equations (78) and (81) indicate a more precise value would be $\pi/2 - \zeta$). The consequence of making dynamic measurements on a high Q system is that there might be some difficulty in practice in measuring the term $M\sin\psi$ accurately.

FREE OSCILLATION DATA REDUCTION PROCEDURE

As an introduction to the data reduction technique a discussion of the principle of least squares (Ref. 4) and the Method of Differential Corrections (Ref. 5) is in order.

The principle of least squares in simple terms states that the curve which best represents a set of data points is the one for which the sum of the squares of the residuals has a minimum value. The term "residual" as referred to in the previous sentence implies a difference between, for a given obscissa, a data ordinate and the curve ordinate (see Figure 6).

If a function $y = f(x,a,b,\ldots)$ is to be fitted to a set of data points (X_i, Y_i), the major problem involves finding values of the constant terms a, b,. . . which will generate the function which will best represent the given data. Application of the least squares principle requires determining the values of a,b,. . . which will make the sum of the residuals squared, ΣV_i^2 , be a minimum. This may be accomplished by developing the set of simultaneously solvable equations,

$$\begin{aligned} \frac{\partial \Sigma V_i^2}{\partial a} &= 0 \\ \frac{\partial \Sigma V_i^2}{\partial b} &= 0 \\ &\vdots \end{aligned} \tag{110}$$

In the function to be fit $f(x,a,b,\ldots)$ is linear in a,b,. . ., then the residual equation (110) will also be linear and the system may be solved with little difficulty. In the functions

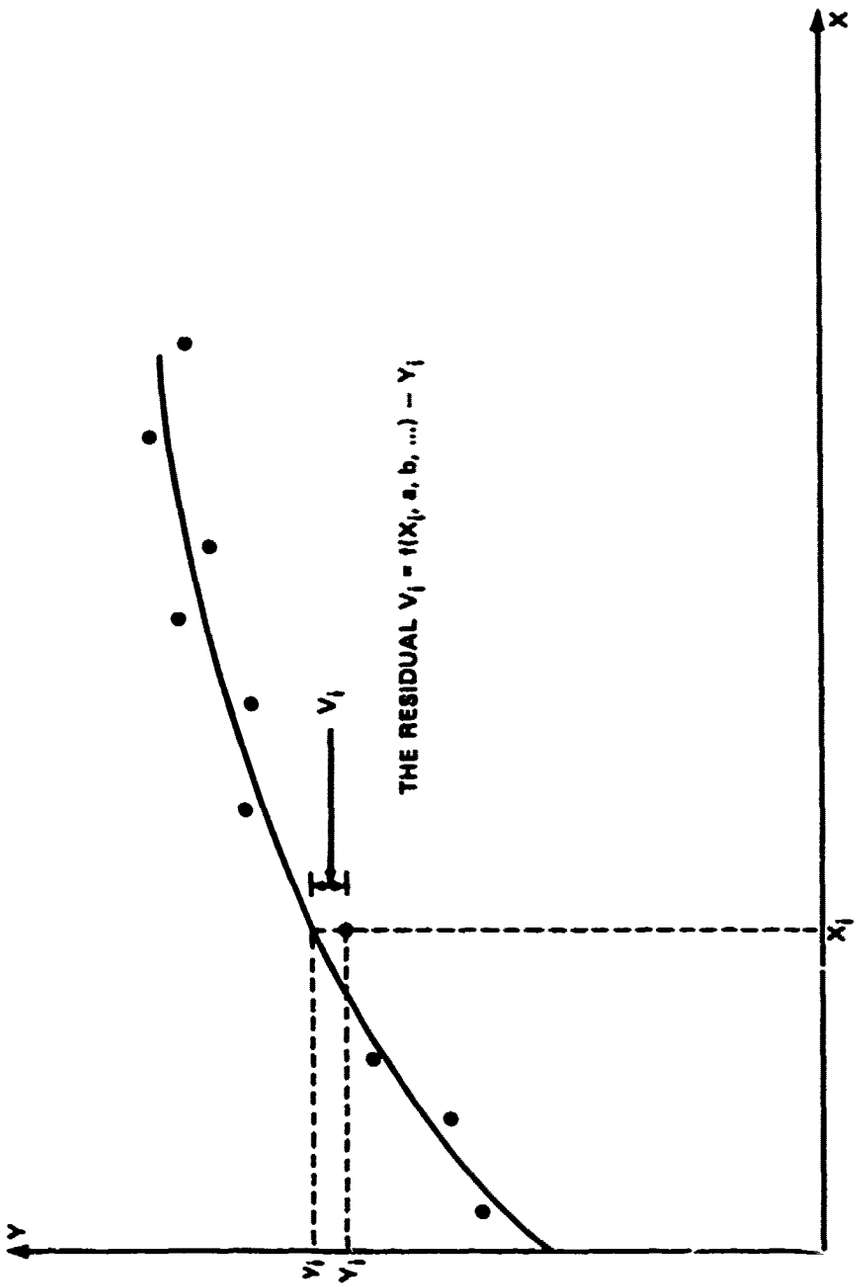

FIG. 6 DEFINITION OF RESIDUAL

which must be used to represent the wind tunnel motions presently being considered, the parameters a,b,. . . are arguments of exponentials, sines, and cosines. Under this requirement the residual equations become non-linear and cannot be directly solved. The Method of Differential Corrections, which will be discussed next, provides an iterative method of solution to any degree of accuracy.

Given a set of N data points (X_i,Y_i) and a function of $y_i=f(x_i,a,b,c)$ which is to be fitted to the data.

The residuals are given by,

$$V_i = f(x_i,a,b,c) - Y_i \tag{111}$$

Let the parameters a, b, and c be defined as follows,

$$\begin{aligned} a &= a_o + \Delta a \\ b &= b_o + \Delta b \\ c &= c_o + \Delta c \end{aligned} \tag{112}$$

where a_o, b_o, and c_o are first approximations of a, b, and c. The problem is not to determine the corrections Δa, Δb, and Δc so that Σv_i^2 is a minimum.

Equation (111) may now be written,

$$Y_i + V_i = f(x_i, a_o+\Delta a, b_o+\Delta b, c_o+\Delta c) \tag{113}$$

Expanding by Taylor's theorem,

$$\begin{aligned} Y_i + V_i = {} & f(x_i,a_o,b_o,c_o) + \Delta a(\partial f_i/\partial a_o) + \\ & \Delta b(\partial f_i/\partial b_o) + \Delta c(\partial f_i/\partial c_o) + (\text{Higher Order terms}) \end{aligned} \tag{114}$$

where f_i means $f(x_i,a_o,b_o,c_o)$.

If the first approximations are reasonably good, the Δ's will be small and the higher order terms may be dropped.

Let us define another residual as the difference between the ordinates of the first approximation curve and the data points,

$$R_i = Y_i - f(x_i,a_o,b_o,c_o)$$

Equation (114) may now be written,

$$V_i = \Delta a\left(\frac{\partial f_i}{\partial a_o}\right) + \Delta b\left(\frac{\partial f_i}{\partial b_o}\right) + \Delta c\left(\frac{\partial f_i}{\partial c_o}\right) - R_i \tag{115}$$

The condition for Σv_i^2 to be a minimum is now,

$$\frac{\partial \Sigma v_i^2}{\partial \Delta a} = 0 \,, \quad \frac{\partial \Sigma v_i^2}{\partial \Delta b} = 0 \,, \quad \frac{\partial \Sigma v_i^2}{\partial \Delta c} = 0 \tag{116}$$

Substituting (115) in (116) and adopting the notation,

$$A_i = \partial f_i / \partial a_o \,, \; B_i = \partial f_i / \partial b_o \,, \; C_i = \partial f_i / \partial c_o$$

$$\begin{aligned} \frac{\partial \Sigma v_i^2}{\partial \Delta a} &= \frac{\partial}{\partial \Delta a} \Sigma (\Delta a A_i + \Delta b B_i + \Delta c C_i - R_i)^2 = 0 \\ &= 2 \Sigma A_i (\Delta a A_i + \Delta b B_i + \Delta c C_i - R_i) = 0 \\ \frac{\partial \Sigma v_i^2}{\partial \Delta b} &= 2 \Sigma B_i (\Delta a A_i + \Delta b B_i + \Delta c C_i - R_i) = 0 \\ \frac{\partial \Sigma v_i^2}{\partial \Delta c} &= 2 \Sigma C_i (\Delta a A_i + \Delta b B_i + \Delta c C_i - R_i) = 0 \end{aligned} \tag{117}$$

where the summations are for i=1,N and N is the number of data points. Expanding eucation (117), dropping the 2's, and writing in matrix form,

$$\begin{bmatrix} \Sigma A_i^2 & \Sigma A_i B_i & \Sigma A_i C_i \\ \Sigma B_i A_i & \Sigma B_i^2 & \Sigma B_i C_i \\ \Sigma C_i A_i & \Sigma C_i B_i & \Sigma C_i^2 \end{bmatrix} \begin{bmatrix} \Delta a \\ \Delta b \\ \Delta c \end{bmatrix} = \begin{bmatrix} \Sigma A_i R_i \\ \Sigma B_i R_i \\ \Sigma C_i R_i \end{bmatrix} \tag{118}$$

Equation (118) are known as the Normal Equations; their solution results in the values of Δa, Δb, and Δc.

Writing equation (115) as a matrix of coefficients and equation (118) as a matrix of coefficients augmented on the right by the column of absolute terms,

$$\begin{bmatrix} A_1 & B_1 & C_1 & R_1 \\ A_2 & B_2 & C_2 & R_2 \\ \cdots & \cdots & \cdots & \cdots \\ A_N & B_N & C_N & R_N \end{bmatrix} \tag{119}$$

$$\begin{bmatrix} \Sigma A_i^2 & \Sigma A_i B_i & \Sigma A_i C_i & \Sigma A_i R_i \\ \Sigma B_i A_i & \Sigma B_i^2 & \Sigma B_i C_i & \Sigma B_i R_i \\ \Sigma C_i A_i & \Sigma C_i B_i & \Sigma C_i^2 & \Sigma C_i R_i \end{bmatrix} \tag{120}$$

A simple algorithm by means of which matrix (120) may be formed directly from matrix (119) is evident: To form the first row of (120) multiply each row of (119) by its own first term and sum the columns; to form the second row of (120), multiply each row of (119) by its own second term and sum the columns; to form the third row of (120), multiply each row of (119) by its own third term and sum the columns.

The residual equation matrix (119) could be very large, since there is a row for each data point. Examination of the above algorithm shows that it is not necessary to generate (119) as a matrix. We may generate the first row of (119), form the necessary products, and add them to the terms of (120) immediately. The first row of (119) may then be replaced by the second row, the necessary products formed, and added to (120); repetition of this process N times produces the complete normal equation matrix (120).

The solution of (120) provides values of Δa, Δb, and Δc. These are used to correct the approximate parameters a_o, b_o, and c_o; these corrected parameters are then taken as improved approximations and the whole procedure repeated. The iteration is continued until there ceases to be significant change in the parameters; the process is then said to have converged.

It is more convenient to test for convergence on a single quantity than on the several parameters. ΣR_i^2 is a suitable quantity; when this ceases to change significantly, the fit is as good as can be achieved.

Equation (13) may be rewritten in the general form,

$$\alpha = Ke^{\lambda t}\cos(\omega t+\phi) + (\alpha_T+\alpha_v) \qquad (121)$$

where the sine and cosine functions differ by a phase angle and the term $\alpha_T+\alpha_v$ account for trim and misalignment of the abscissa of the data acquisition system and the velocity vector. In the fitting procedure $\alpha_T+\alpha_v$ cannot be determined separately so a single factor $K_2=(\alpha_T+\alpha_v)$ is determined. Equation (121) is the fitting model which is utilized to represent the one-degree-of-freedom motion.

The independent variable of the fitting model is time. The data is assumed to consist of corresponding values of missile attitude angle and time. The method of differential corrections imposes no inherent requirement for a constant time interval. Data, however, is usually presented in terms of a constant time interval, and great simplification of logic results where fitting is done with respect to a uniform scale.

K and ϕ are the magnitude and orientation of a vector arm at t=0. If a section of data late in a flight or wind tunnel run is fitted in terms of real time, K and ϕ will be extrapolated back to zero time in accordance with the current values of λ and ω. It is therefore incident that the time array should be normalized so that zero time is located within the section of data being fitted.

Wind tunnel data are always at least slightly non-linear; that is, λ and ω change somewhat with time. The values of λ and ω obtained by fitting a linear model to such data are mean values related to the mean or middle time of the section of data being fitted. Since K and ϕ are related to zero time, the time array should be normalized so that zero time is at the middle of the section of data being fitted; all parameters will then be obtained related to the same instant of time.

The parameters to be determined by fitting the model to the data are K, λ, ω, ϕ, and K_3. Reasonably good first approximations of these quantities are necessary to start the differential corrections procedure. The final results do not depend upon the accuracy of these approximations; the only requirement is that they be good enough to result in a convergent iteration. These first approximations are illustrated in Figure 7.

K_3 may be determined as the mean of the two extreme points of minimum amplitude.

ω may be determined from, $\omega = \frac{(n-1)}{t_n}\pi$, where n is the number of extreme points and t_n is the time interval between the first and last of the extreme points.

ϕ may be determined as $\phi = \omega t_\phi$, where t_ϕ is the time interval between the normalized time zero (middle point of section of data being fitted) and the preceding positive maximum. A poor first approximation may result in a negative value for K; the absolute value will be correct, however.

K is determined as the distance from the K_3 line to the intercept at normalized time zero of the envelope of positive maximum points.

λ=0 will usually provide a reasonable first guess for the λ term.

The maximum allowable error in the approximation of ω depends upon the resulting maximum phase difference between the model and the data. For a given error in ω, the phase difference is proportional to the number of cycles included in the section of data being fitted; therefore, greater accuracy is required when fitting a long section of data.

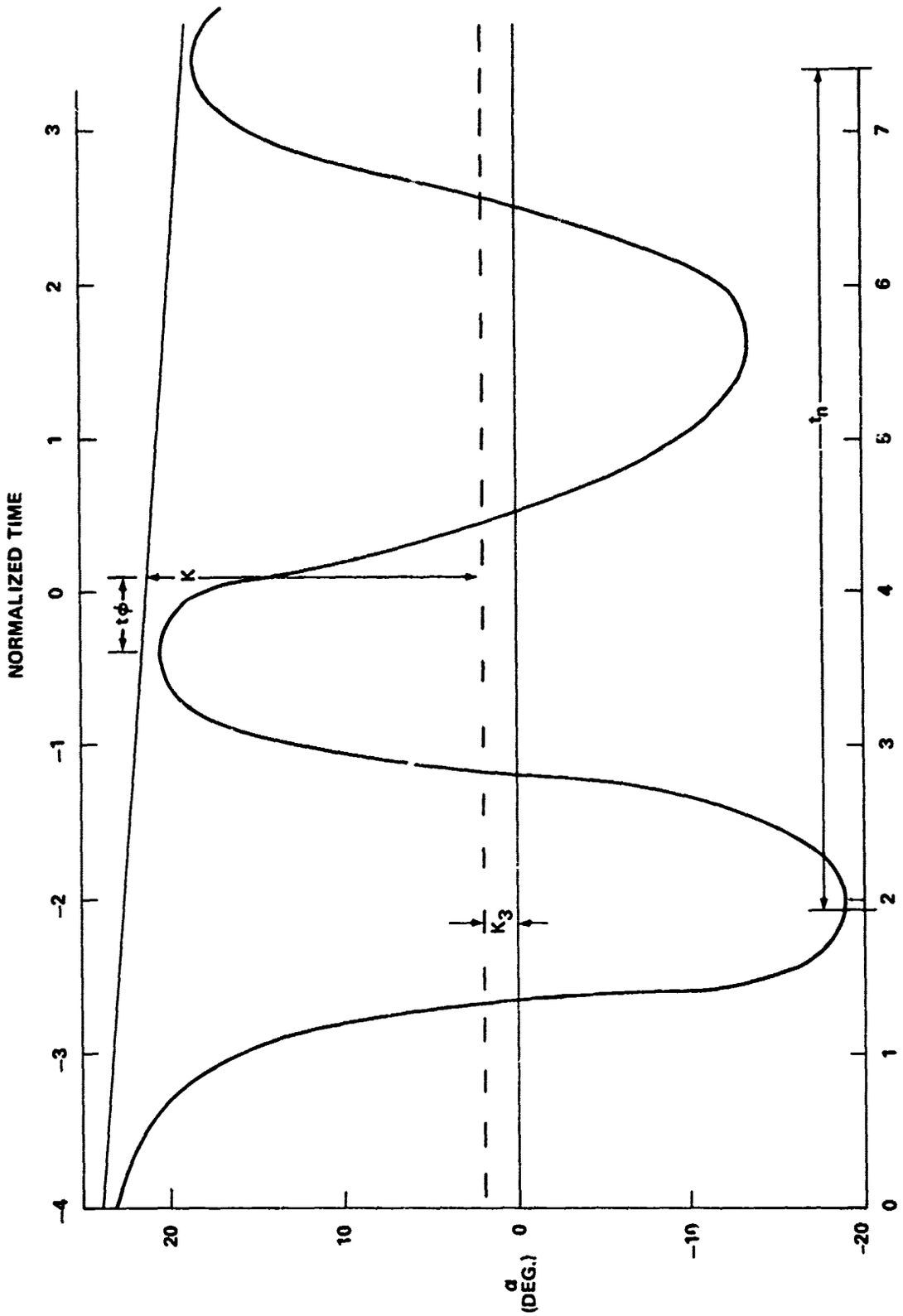

FIG. 7 FIRST APPROXIMATIONS

The derivatives required to form the residual equations can now be expressed as,

$$
\begin{aligned}
A_i &= \frac{\partial \alpha_i}{\partial K_3} = 1 \\
B_i &= \frac{\partial \alpha_i}{\partial K} = e^{\lambda t_i} \cos(\omega t_i + \phi) \\
C_i &= K t_i B_i \\
D_i &= \frac{\partial \alpha_i}{\partial \phi} = -K e^{\lambda t_i} \sin(\omega t_i + \phi) \\
E_i &= \frac{\partial \alpha_i}{\partial \omega} = t_i D_i \\
R_i &= \alpha_i - [K e^{\lambda t_i} \cos(\omega t_i + \phi) + K_3]
\end{aligned}
\qquad (122)
$$

The normal equation matrix differs from equation (120) only in the addition of two rows and columns for the additional derivatives D and E. The summations of equation (120) are for i=1 to N where N is the number of data points to be fitted.

Following is a listing of a FORTRAN IV subroutine which has been used to fit the data of the current discussion.

```
      PROGRAM CARDAMP(INPUT,OUTPUT,TAPE5=INPUT,TAPE6=OUTPUT,TAPE76,
     1TAPE1,TAPE2,TAPE99)
      DIMENSION CO(6000,1),LABEL(50),TIME(6000),A(26,3)
      READ(5,10) KRUN
      IF(KRUN.NE.0)READ(5,10)(LABEL(I),I=1,KRUN)
   10 FORMAT(24I3)
      CALL EDIT(CO,2000,6000,KRUN,LABEL)
      DO 500  N7=1,3
      READ(5,11) TBEG,TEND
   11 FORMAT(2F12.6)
      READ(1) IWIND,NS,ISA,IEA,NA,JFRMS,JFRMSZ,JBLSZ,NRUN
      IF(JFRMS.GT.6000) STOP1
      READ(1)((CO(L,K),K=1,NA),L=1,JFRMS)
      JFRMS=JFRMS-1
      LCN=0
      IBD=1
      DO 55  L=1,JFRMS
      IF(L.EQ.1) TIME(L)=0.0
      IF(L.GT.1) TIME(L)=TIME(L-1)+.004
      IF((TIME(L).LT.TBEG).OR.(TIME(L).GT.TEND)) GO TO 55
      LCN=LCN+1
      IF(LCN.EQ.1) TIME(LCN)=0.0
      IF(LCN.GT.1) TIME(LCN)=TIME(LCN-1)+.004
      CO(LCN,1)=CO(L,1)
   55 CONTINUE
      JFRMS=LCN
      CALL VALUE(NRUN,JFRMS,TIME,CO,A,IWD,CAT,TBEG,TEND)
      JFRMS=400
      CALL FIT(NRUN,JFRMS,TIME,CO,LCN,A,CAT)
  500 CONTINUE
      STOP
       END
```

```
      SUBROUTINE VALUE(NRUN,JFREQS,TIME,CC,A,IND,CNT,TBEG,TEND)
      DIMENSION CC(6000,1),TIME(6000),PMAX(25),TMAX(25),PMIN(25),TMIN(25
     1),A(26,3)
      LMIN=1
      LMAX=1
      XMIN=0.0
      XMAX=0.0
      DO 10 J=2,JFREQS
      IF(CC(J,1).LT.CC(J-1,1)) XMAX=XMAX+1.0
      IF(XMAX.EQ.1.0) PMAX(LMAX)=CC(J-1,1)
      IF(XMAX.EQ.1.0) TMAX(LMAX)=TIME(J-1)
      IF(XMAX.EQ.1.0) LMAX=LMAX+1
      IF(LMAX.EQ.12) GO TO 15
      IF(J.EQ.2) LMAX=1
      IF(XMAX.EQ.1.0) XMIN=0.0
      IF(CC(J,1).GT.CC(J-1,1)) XMIN=XMIN+1.0
      IF(XMIN.EQ.1.0) PMIN(LMIN)=CC(J-1,1)
      IF(XMIN.EQ.1.0) TMIN(LMIN)=TIME(J-1)
      IF(XMIN.EQ.1.0) LMIN=LMIN+1
      IF(J.EQ.2) LMIN=1
      IF(XMIN.EQ.1.0) XMAX=0.0
   10 CONTINUE
   15 IF(IND.EQ.1) WRITE(6,59) NRUN
   59 FORMAT(1H1,10X,4HRUN ,I3,10X,6HMIND OFF//)
      IF(IND.EQ.2) WRITE(6,58) NRUN
   58 FORMAT(1H1,10X,4HRUN ,I3,10X,7HMIND ON//)
      WRITE(6,101) TBEG,TEND
      WRITE(6,100)(PMAX(I),I=1,9)
      WRITE(6,101)(TMAX(I),I=1,9)
      WRITE(6,100)(PMIN(I),I=1,9)
      WRITE(6,101)(TMIN(I),I=1,9)
  100 FORMAT(10F10.1)
  101 FORMAT(10F10.3)
      CNT=TMAX(1)
      A(5,1)=(PMAX(1)+PMIN(1))/2.0
      A(4,1)=1.571
      FREQ=(TMAX( 9)-TMAX(1))/8.0
      A(3,1)=6.28318/FREQ
      A(2,1)=PMAX(1)-A(5,1)
      ANUM=PMAX(1)-PMAX(9)
      DENM=(TMAX( 9)-TMAX(1))*(PMAX(9)-A(5,1))
      A(1,1)=ANUM/DENM
      WRITE(6,50) NRUN,(A(I,1),I=1,5),CNT
   50 FORMAT(I5,6F10.3)
      RETURN
       END
```

```
      SUBROUTINE FIT(NPLN,JFRMS,TIME,CC,LCN,A,CNT)
      DIMENSION N(5),X(5,4000),A(26,3),CC(4000,1),TIME(4000)
      EXTERNAL VF
      NPAR=5
      N(1)=NPAR
      N(2)=JFRMS
      N(3)=2
      N(4)=1
      N(5)=0
      DO 10 I=1,NPAR
   10 A(I,3)=I
      DO 20  L=1,JFRMS
      X(1,L)=TIME(L)-CNT
      X(2,L)=CC(L,1)
   20 CONTINUE
      DELT=1.0E-6
      DO 777 NPASS=1,50
      IF(NPASS.EQ.12) RETURN
      CALL LSQSUB(N,X,A,VF,DELT)
      IF(A(26,1).GT.0.) GO TO 62
      WRITE(6,60)      (A(I,1),I=1,NPAR),A(26,1),A(26,2),A(26,3)
   60 FORMAT(   8F14.7/5E14.7/)
      IF(A(1,1).LT.0.0) RETURN
  777 CONTINUE
   62 WRITE(6,60) (A(I,1),I=1,NPAR),A(26,1),A(26,2),A(26,3),
     1(A(I,2),I=1,NPAR)
      N(2)=MIN0(LCN,4000)
      JFRMS=MIN0(LCN,4000)
      DO 11  I=1,NPAR
   11 A(I,3)=1
      DO 21  L=1,JFRMS
      X(1,L)=TIME(L)-CNT
      X(2,L)=CC(L,1)
   21 CONTINUE
      DO 778  NPASS=1,50
      IF(NPASS.EQ.12) RETURN
      CALL LSQSUB(N,X,A,VF,DELT)
      IF(A(26,1).GT.0.) GO TO 63
      WRITE(6,60)      (A(I,1),I=1,NPAR),A(26,1),A(26,2),A(26,3)
      IF(A(1,1).LT.0.0) RETURN
  778 CONTINUE
   63 WRITE(6,60) (A(I,1),I=1,NPAR),A(26,1),A(26,2),A(26,3),
     1(A(I,2),I=1,NPAR)
   65 DO 25  K=1,JFRMS
      CO(K,1)=EXP(-A(1,1)*(TIME(K)-CNT))*A(2,1)*SIN(A(3,1)*(TIME(K)-CNT)
     1+A(4,1)))+A(5)
```

```
 25 CONTINUE
    SUM1=0.0
    WRITE(6,200)
200 FORMAT(//*  RLN          TIME     TIME-CAL.        INPUT            CALC
   1          DIFF*)
    DO 30  K=1,JFRMS
    DIFF=CO(K,1)-X(2,K)
    SUM1=SUM1+DIFF**2
 30 CONTINUE
    DEV=SQRT(SUM1/JFRMS)
    WRITE(6,101) DEV
101 FORMAT(E14.7)
    DO 31  K=1,JFRMS,20
    DIFF=CO(K,1)-X(2,K)
    TIM=TIME(K)-CAT
    WRITE(6,100) KRLN,TIME(K),TIM,X(2,K),CO(K,1),DIFF
100 FORMAT(I5,2F12.3,3F14.7)
 31 CONTINUE
    RETURN
     END
     END
```

```
      SUBROUTINE VF(N,X,DF,A)
      DIMENSION DF(1),X(1),A(1),N(1)
C  EQUATION TO FIT.... F=EXP(-A(1)*X)*A(2)*SIN(A(3)*X+A(4))+A(5)
C           ..... X = TIME-SHIFT CONSTANT .....
      SA3=SIN(A(3)*X(1)+A(4))
      EA1=EXP(-A(1)*X(1))
      DUM =EA1*A(2)*SA3
      DF(2)=EA1*SA3
      DF(1)=-X(1)*DUM
      SUM  =A(2)*EA1*COS(A(3)*X(1)+A(4))
      DF(3)=X(1)*SUM
      DF(4)=SUM
      DF(5)=1.
      X(9)=DUM+A(5)
      RETURN
       END
```

THE SMALL-AMPLITUDE FREE-OSCILLATION SYSTEM

The Supersonic Tunnel Association standard ten degree cone was selected as the test configuration. The model has interchangable nose sections which resulted in bluntnesses of .0167, .1, and .25 when moted with the conical afterbody which had a 4.5 inch diameter base. Several ballast rings are located in the model near its base to ensure proper static balancing. The forward end of the cone was fit with a ring holder which attached the cone to the flexure mount of the supporting sting. The cone, noses, flexure ring holder, and a sample ballast ring are shown in Figure 8.

The basic components of the sting support and model system are illustrated in Figure 9. The sting is designed to permit the attachment of seven commerically available torsional flexure mounts to allow for a variety of torsional stiffness and load carrying characteristics, which may be required to meet a specific test objective. For the present test 5/8 inch cross flexures of spring constants of K=106.0 and 13.3 inch-lbs/radian were selected. Using flexures of differing spring constants allows evaluation of frequency effects.

The model-sting system is injected into the flow field at the desired sting angle-of-attack. Secondary oscillation of the support system initially appeared to be a problem. To alleviate this problem the angle-of-attack servo mechanism is clamped to the wind tunnel superstructure. An initial angle-of-attack and the subsequent resulting small oscillations about the stirg angle-of-attack is achieved by a pneumatically actuated piston, rod, and tripping lever system. Application of air pressure to the rear of the piston drives the piston and rod forward causing the tripping lever to rotate outward and contact the model. The model is caused to rotate about the flexural pivot point, with the maximum deflection angle being dependent on the height of the lever hammer head. As the piston moves further forward, the level is quickly released which allows the model to freely oscillate about the pivot point. Application of air pressure on the other side of the piston retracts the actuating rod and sets the system for another triggering sequence. Several trips may be achieved during each wind tunnel run, allowing several damping records to be obtained. A data record is also obtained prior to and just after a wind tunnel run to allow determination of tare damping values under near vacuum conditions.

In order to sense and continuously read out the instantaneous model attitude, the cross members of the flexure pivot are instrumented with a dual, heat conpensating, strain gage system. Such a system provides a back-up gage in the event of a failure of the main system. The strain gage flexure system was thoroughly investigated to ensure that there was no increased structural damping or thermal sensitivity associated with the installation of the strain gages on the flexural members. In the present application, the

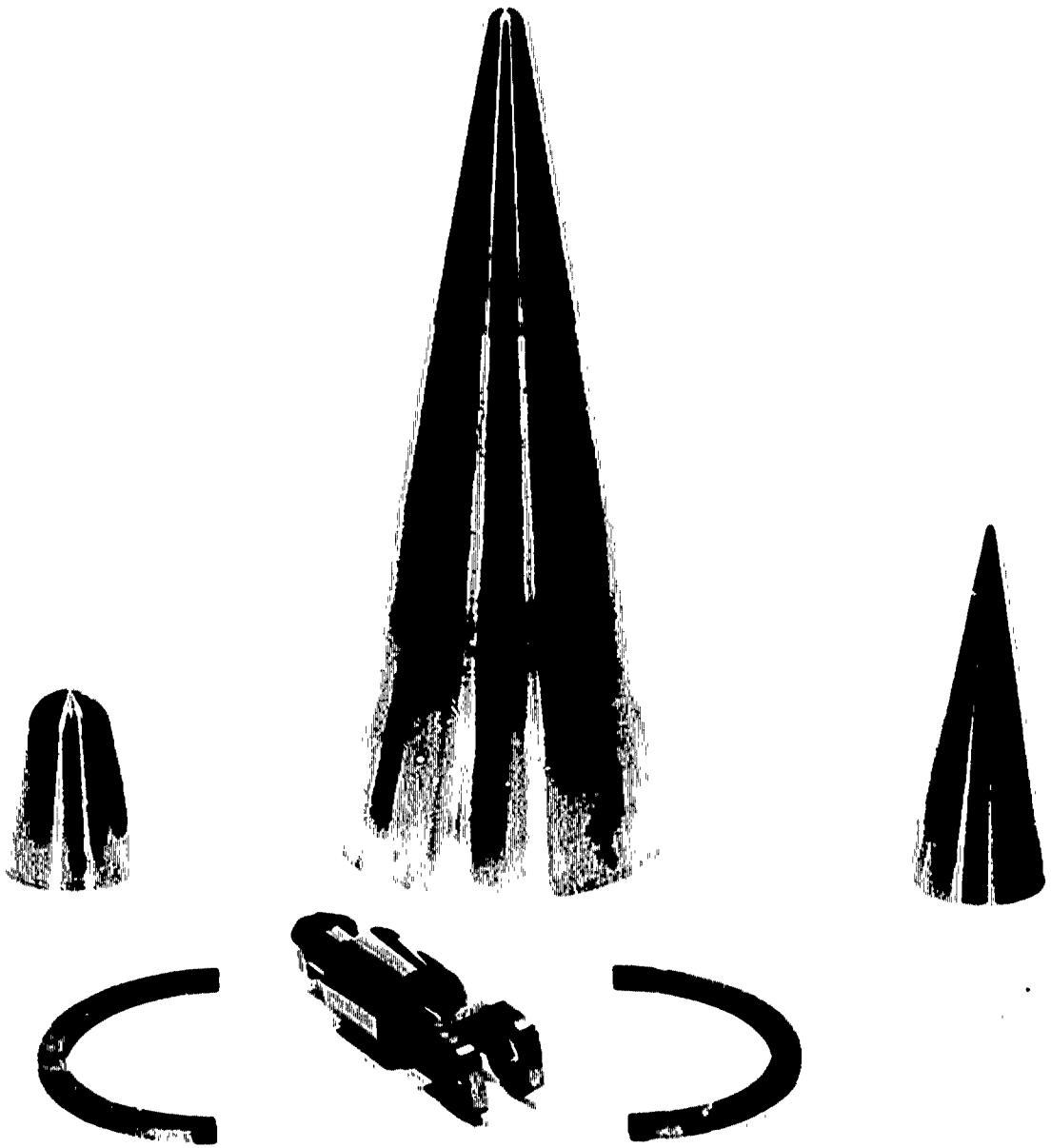

FIG. 8 TEST CONFIGURATION AND FLEXURE SUPPORT

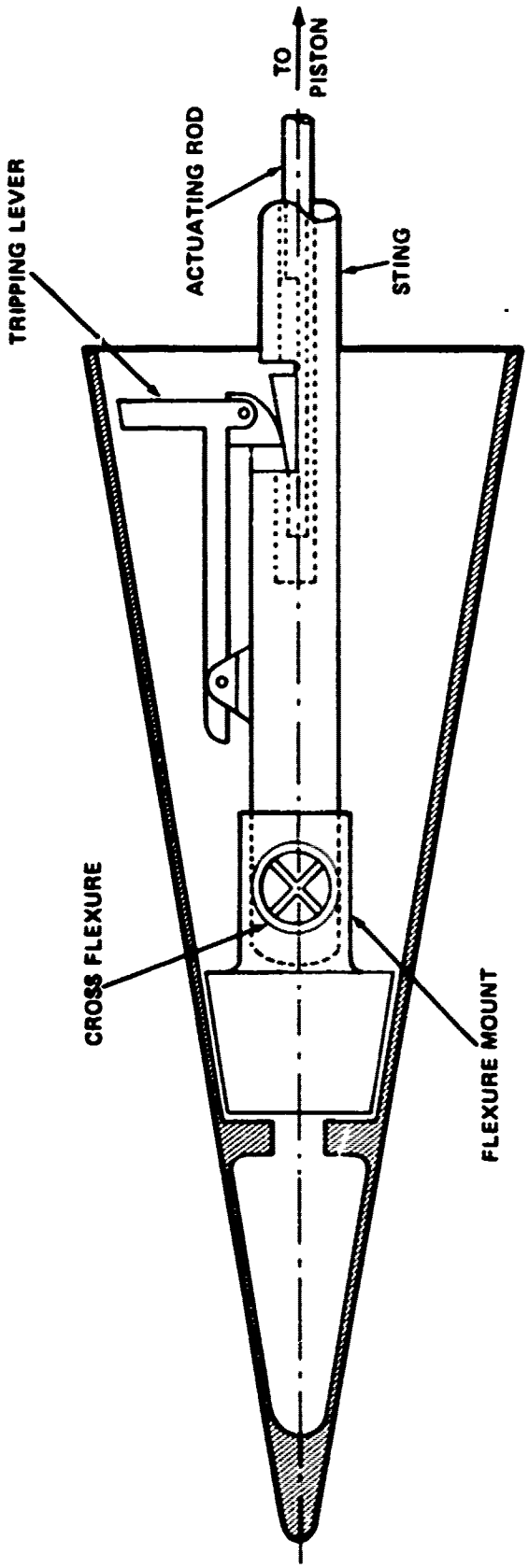

FIG. 9A FREE-OSCILLATION STING AND FLEXURE SCHEMATIC

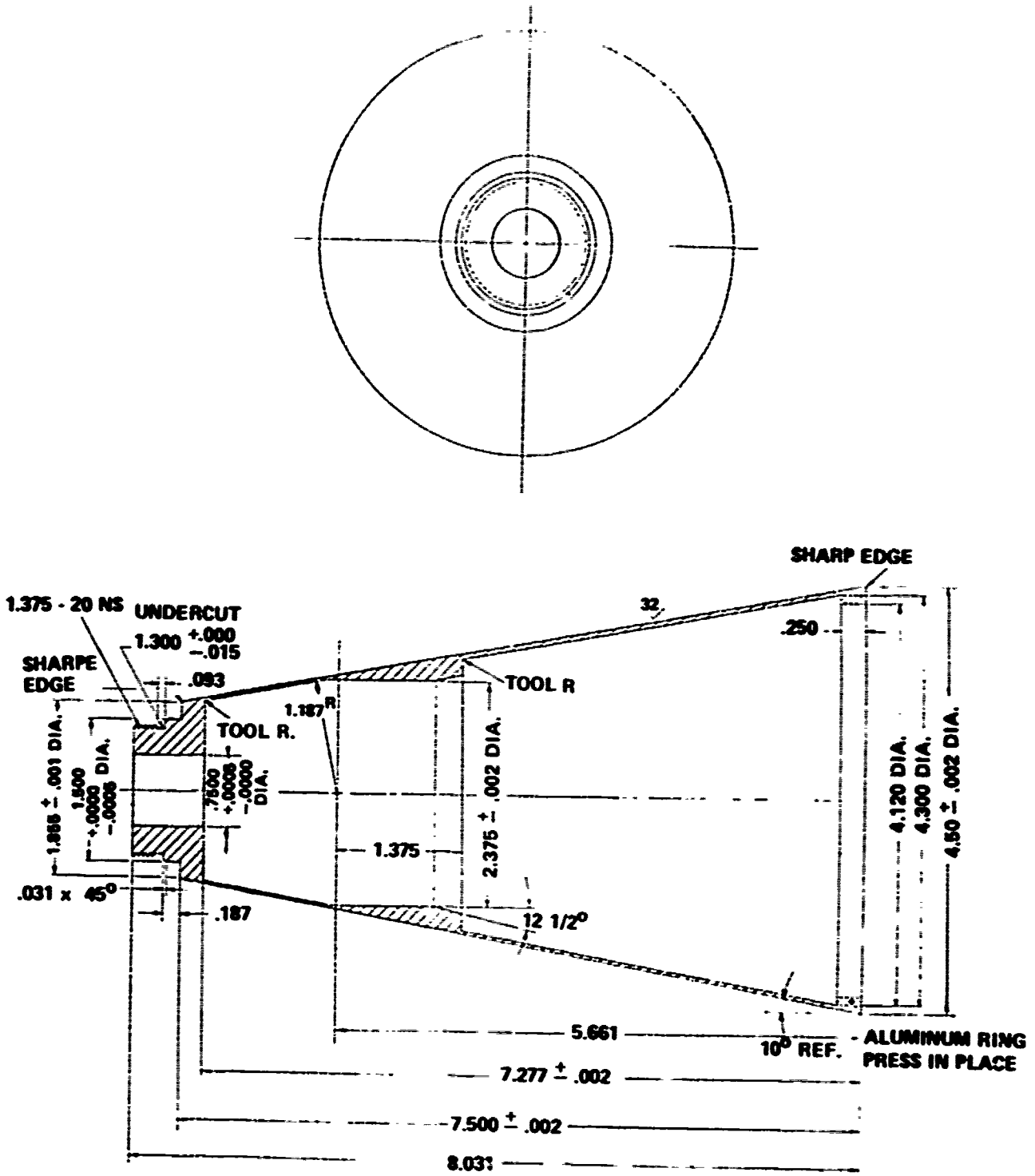

FIG. 9B MODEL BODY

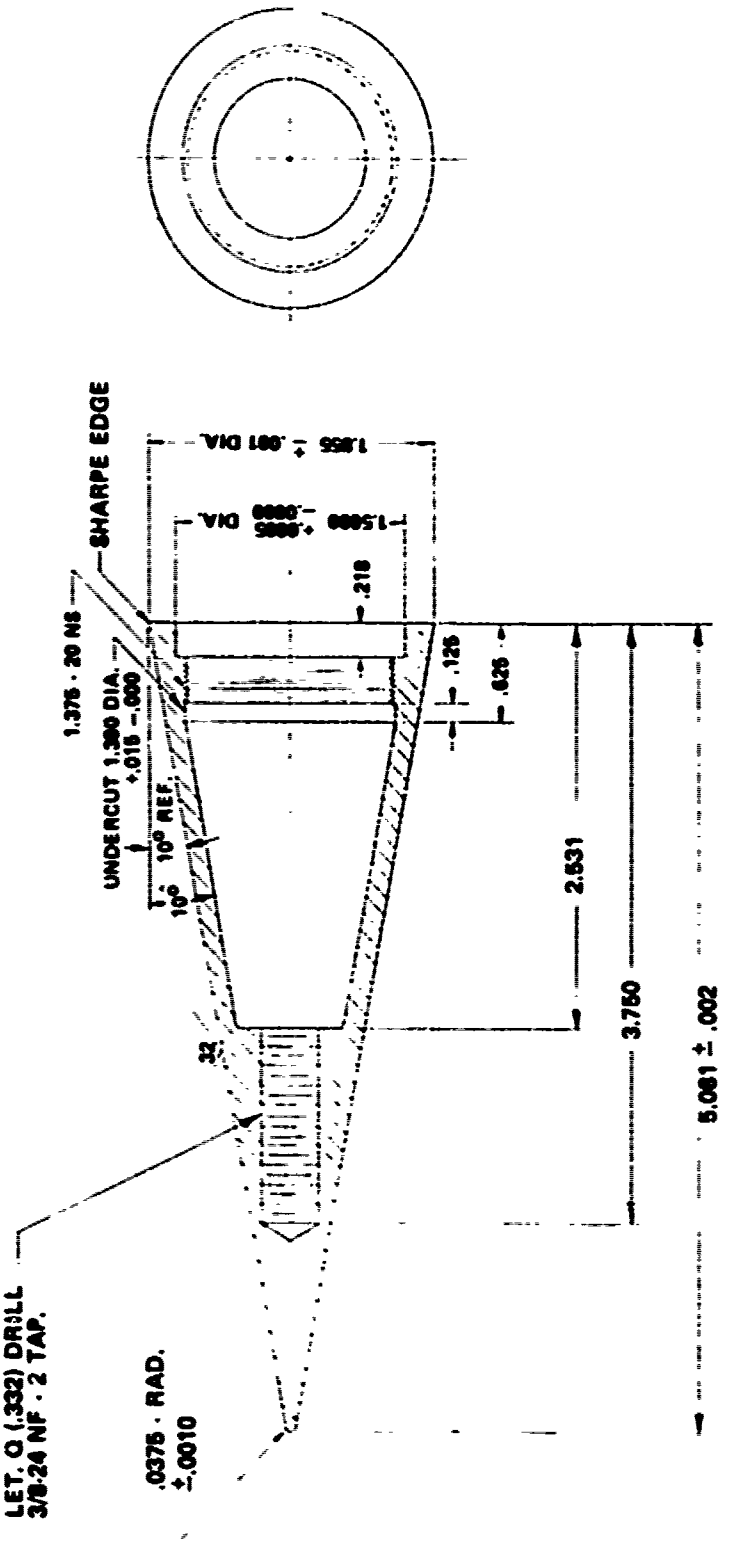

FIG. 9C MODEL NOSE

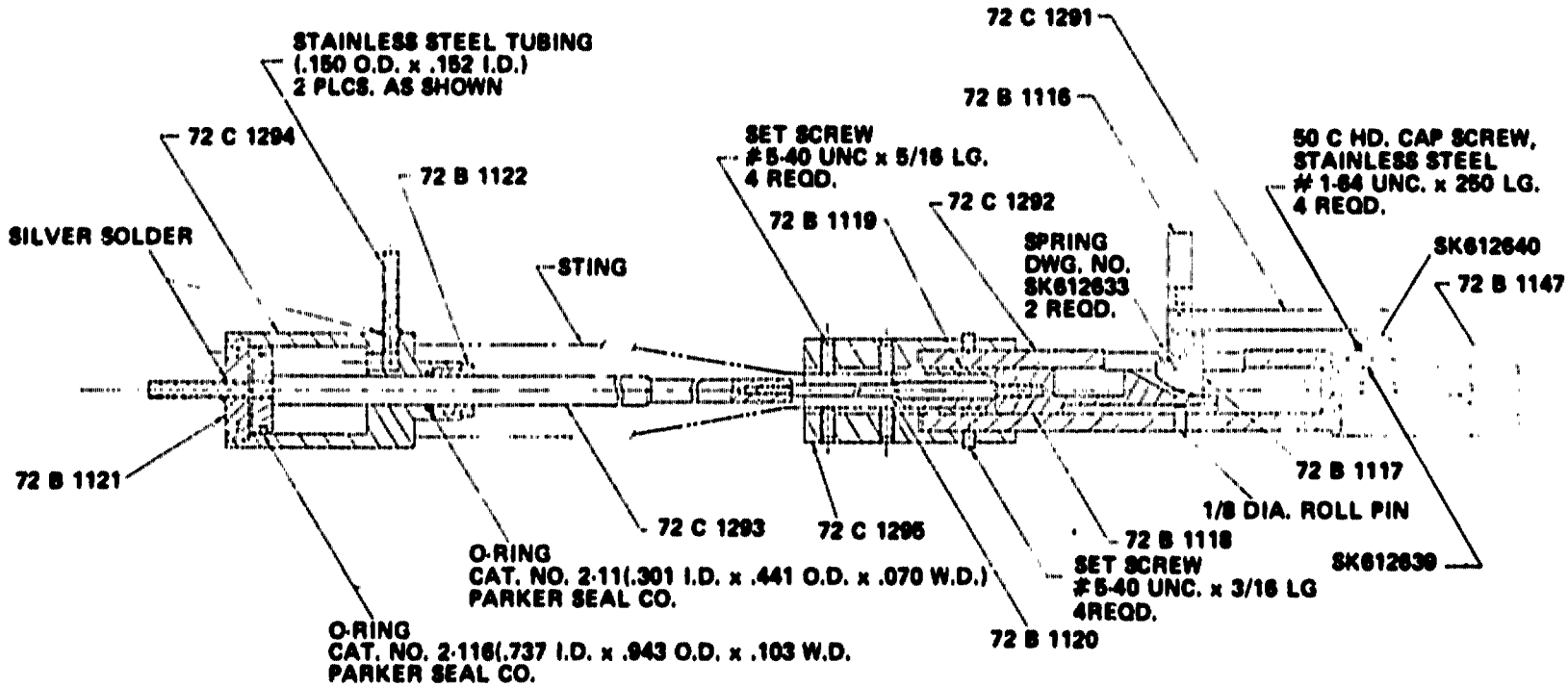

FIG. 9D STING ASSEMBLY

system output is suitably filtered and recorded on magnetic tape for later analysis. The system was also calibrated to provide displacement, system unit conversion factors. At the highest sampling rate available the present data acquisition and recording system storage memory fills to capacity in about two seconds, and this data must then be transferred to magnetic tape, an operation requiring about one second. Hence, either an interrupted record of the model angle-of-attack history of approximately 10 to 20 seconds duration is obtained from a single triggering of the model, or a series of records of two-second duration initiated by repeat triggers the model during the data transfer intervals is obtained for analysis. Both procedures appear useful for typical model oscillation frequencies in the neighborhood of 5 to 15 hertz. A schematic representation of the signal path is presented in Figure 10. The lead cables from the strain gages are blanketed and taped to the sting to provide insulated and prolution. This process results in a maximum sting diameter of 2 inches, 14 inches downstream of the model base and a sting diameter of 1-1/4 inches immediately aft of the model base. The model and blanketed and taped sting are shown in Figure 11. An oscilloscope provides a means of continuous monitoring of the movement of the model.

The torsional pendulum method was used to determine the transverse moment of inertia of the various configurations of the model after each configuration had been statically balanced. Using the torsional technique, the inertial moments were first computed for a test mass of known density and cross section. These results were then compared to computer moments of inertia with errors of small magnitude resulting. The accuracy of the experimental results was thereby confirmed. Results of the torsional technique for the three statically balanced configurations of the model are presented below for a center of gravity located 4.466 inches from the base of the model.

R_n/R_B	I (slug-ft^2)
.0167	7.985×10^{-3}
.1	7.452×10^{-3}
.25	6.403×10^{-3}

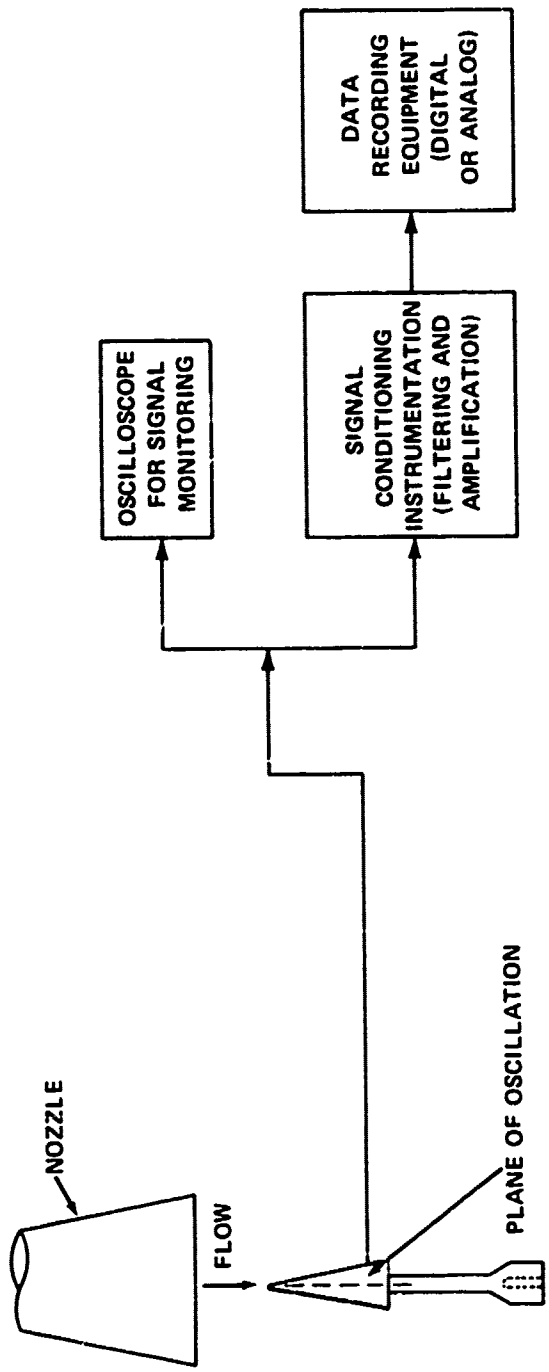

FIG. 10 SCHEMATIC OF SIGNAL PATH

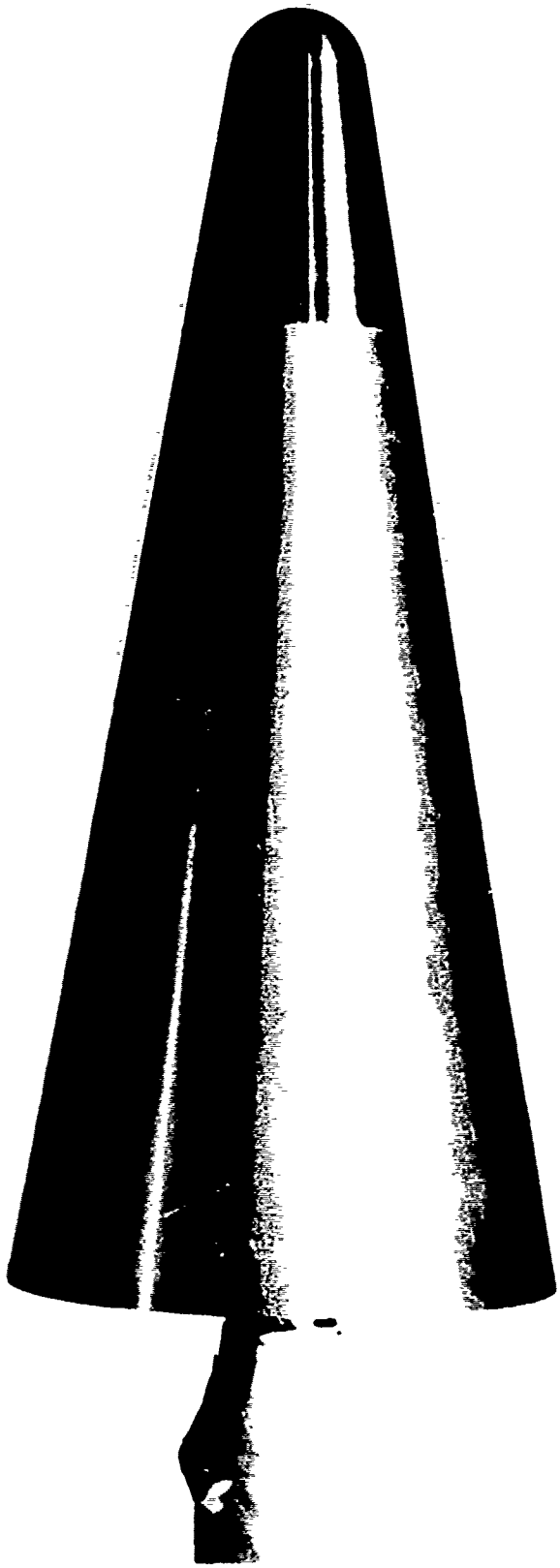

FIG. 11 - Model and Support Sting Mounted in Hypervelocity Research Tunnel

FORCE OSCILLATION SYSTEM

The forced-oscillation technique is based on the principle that when a simple mechanical system is externally forced to oscillate near its undamped natural frequency,* the input force (or moment) required to maintain the motion is just that necessary to overcome the inherent damping in the system (Ref. 2). Hence a measurement of the forcing function is equivalent to a measurement of the system damping. In theory, the oscillation need not be exactly at the resonant frequency, as a measurement of the forcing function and phase difference between the input force (or moment) and the system response is sufficient to provide a means for deducing the damping. However, in practice, the technique becomes less useful as the oscillation frequency departs from the system natural frequency, and most forced-oscillation damping measurement systems operate at or near resonant conditions.

The forced-oscillation mechanism used is illustrated in simplified from in Figure 12. The model is attached to the pivoting head, which is forced to perform a single-degree-of-freedom oscillation about the pivot point by a yoke and eccentric crank attached to a rotating shaft driven by a one-third horsepower universal motor located in the drive-unit housing, as indicated.

The balance, designed and built at the NASA Langley Research Center for a hypersonic free-jet wind tunnel, employs the 90-degree drive shaft turn in order to minimize undesirable tunnel blockage and heating effects which would result from a motor housing mount located on the sting axis. Oscillation frequencies from about one to 50 hertz can be obtained and oscillation amplitudes up to two degrees can be generated by the currently available components. Operation of the balance is restricted to maintaining the plane of oscillation coincident with a vertical plane, although the balance may be pitched either up or down to a maximum angle of 30 degrees and may be yawed to angles restricted only by load limitations on the balance head. Hence, in-plane damping is achieved by pitching the balance in the oscillation plane, and out-of-plane damping is obtained by yawing the balance normal to the oscillation plane.

---

*Resonance occurs from equation (72) when

$$\omega_f = \omega_n \sqrt{1-2\zeta^2} \approx \omega_n (1-\zeta^2)$$

and

$$\omega_d = \omega_n \sqrt{1-\zeta^2}$$

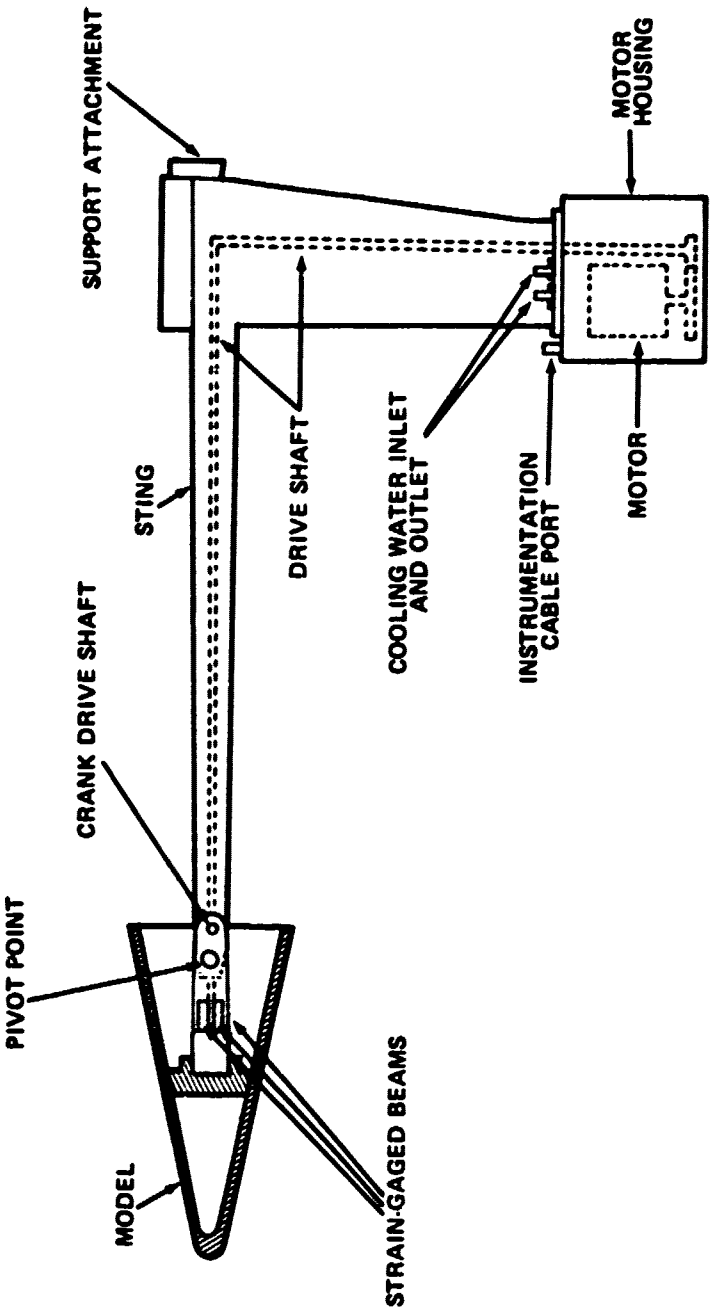

FIG. 12 FORCED-OSCILLATION BALANCE SCHEMATIC

Loads transmitted to the model are deduced from strain-gage measurements on the upper and lower beams shown in Figure 13, which schematically illustrates the forward balance arrangement. This moment beam design was selected to provide maximum strain (i.e., gage response) with minimum deflection so that the model is rigidly forced to perform the motion generated by the shaft crank and yoke. The degree to which this is achieved is related to the ratio of oscillation frequency to the mechanical natural frequency of the moment beam and mass located forward of the beam. Note will be made of this point when balance calibration and data reduction are discussed. It is also important to note that the moment beam is located between the pivot and the model, and therefore loads measured by the gages located thereon do not contain drive-train or pivot frictional components.

The instantaneous angular displacement of the model relative to the sting is obtained from strain gages mounted on the center deflection beam mounted between the model and the sting, as illustrated in Figure 13. The stiffness of this beam and the inertia of the model and pivoting head combine to generate a natural oscillation frequency of the balance and model. This frequency is changed by the addition of aerodynamic stiffness during wind-tunnel flow conditions, but typically the deflection beam stiffness is greater than the aerodynamic stiffness, as operation at as high a value of reduced frequency as possible is usually desirable. This maximum frequency is limited by the minimum model moment of inertia which can be practically obtained and by the maximum frequency allowable by both the data-acquisition system and by the dynamic characteristics of the balance itself. A foil strain-gage bridge is mounted on the defelction beam, whereas semiconductor strain gages are mounted on the moment beams to provide increased sensitivity.

In order to obtain satisfactory performance under high-temperature hypersonic tunnel flow conditions, the balance is provided with water cooling. However, water cooling passages are not provided within the strain-gage beams due to size limitations, and these elements can be subjected to some temperature draft during testing. The bridges are temperature compensated and, in addition, since oscillation signals are the primary measurement objective, a slow bridge-zero drift due to uneven thermal loading can be eliminated by monitoring only the a.c. component of the bridge outputs. This technique does not account for bridge sensitivity changes due to uniform temperature changes; however, account can be taken of the latter by calibration and by appropriate design technique.

It is also desirable that the pitching-moment reference point be located at the oscillation pivot point. As shown in Figure 13, however, the pitching-moment beam is located some distance forward of the pivot point. Additional strain-gage

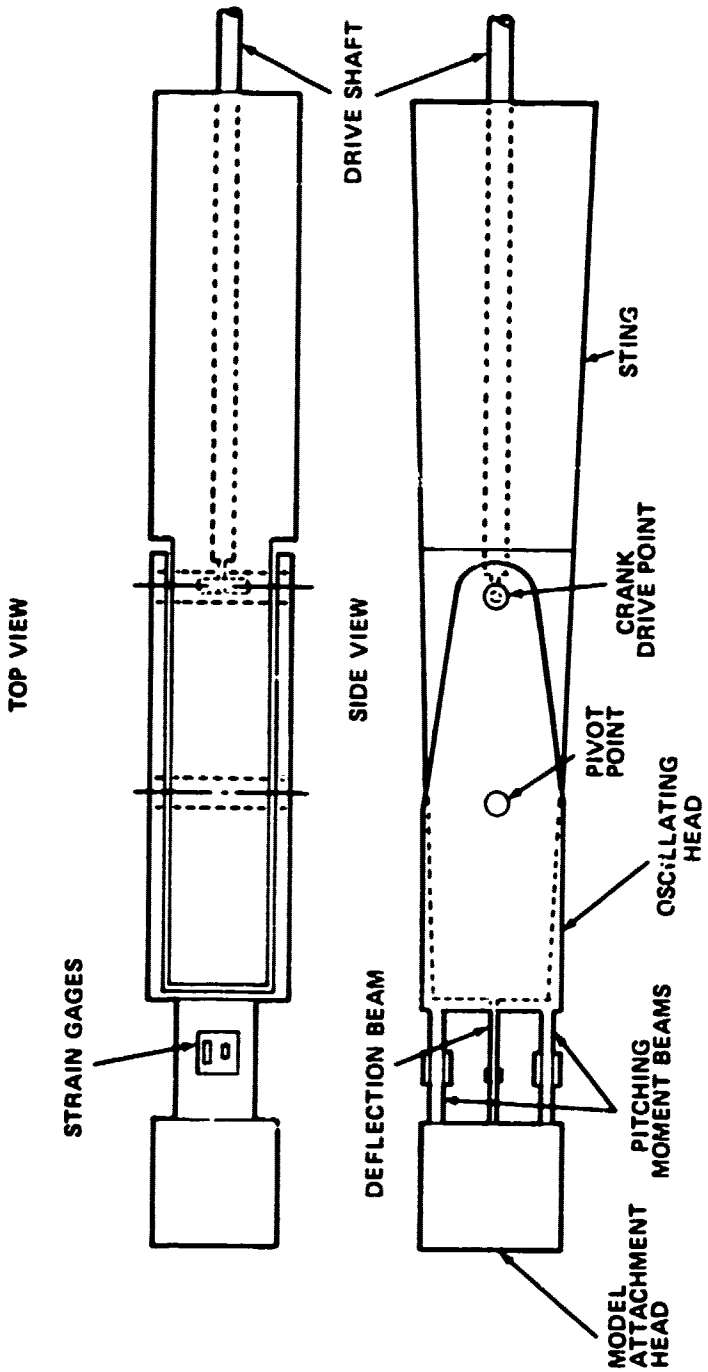

FIG. 13 FORCED-OSCILLATION BALANCE HEAD DETAIL

bridges are provided on the beam elements to develop a normal-force signal, which is subsequently combined with the pitching moment, analogous to a simple moment-transfer equation, to yield an output moment signal referenced about the pivot point. This signal combination is accomplished on the balance itself.

Calibration of the balance and associated read-out instrumentation requires consideration of both static and dynamic effects. Static calibration was accomplished in a conventional manner by dead-weight loading with d.c. bridge excitation voltages of 2, 4, 5, and 7 volts. Actual operation of the balance was performed with a bridge voltage of approximately 4 volts.

It is important to note that the pitching-moment beam deflections under actual oscillating conditions represent dynamic deflections and, as such, require smaller loads for equal strains than under equivalent static conditions. That is, the instantaneous beam deflection is a function of applied load and frequency, and in principle a dynamic calibration at several oscillation frequencies is required. In practice, one normally assumes that the mechanical natural frequency of the moment beam and model inertia combination is very much higher than the oscillation frequency during testing, and hence the dynamic deflections can be expected to be approximately equal to static deflections under equal loading.

An indication of the relative dynamic amplification has been obtained by earlier tests performed on the balance for NASA. A sketch of the test setup for that study is shown in Figure 14. Sinusoidal loads were generated by an electro-mechanical shaker and applied to the balance through a calibration fixture. The fixture served as an inertia load and as a means for load application. A load amplitude of two poinds was maintained while the frequency was varied from 1 to 160 hertz. The balance strain-gage bridge outputs were recorded and analyzed to provide the frequency response characteristics of the balance-fixture system. The output from each bridge was normalized to the one hertz reference value.

Figure 15 shows a representative frequency response curve for the pitching-moment bridge output as a function of load frequency. A resonant frequency of about 45 hertz can be observed with the dynamic response amplification being about 10 at this frequency. Note that at a frequency of about 10 hertz, the output is approximately 10 percent higher than the static value. Therefore, during actual testing at this frequency, one would reduce the output measurement about 10 percent in order to obtain the actual load magnitude from static calibration information. This result is, of course, dependent on the fixture inertia characteristics being representative of the actual model characteristics.

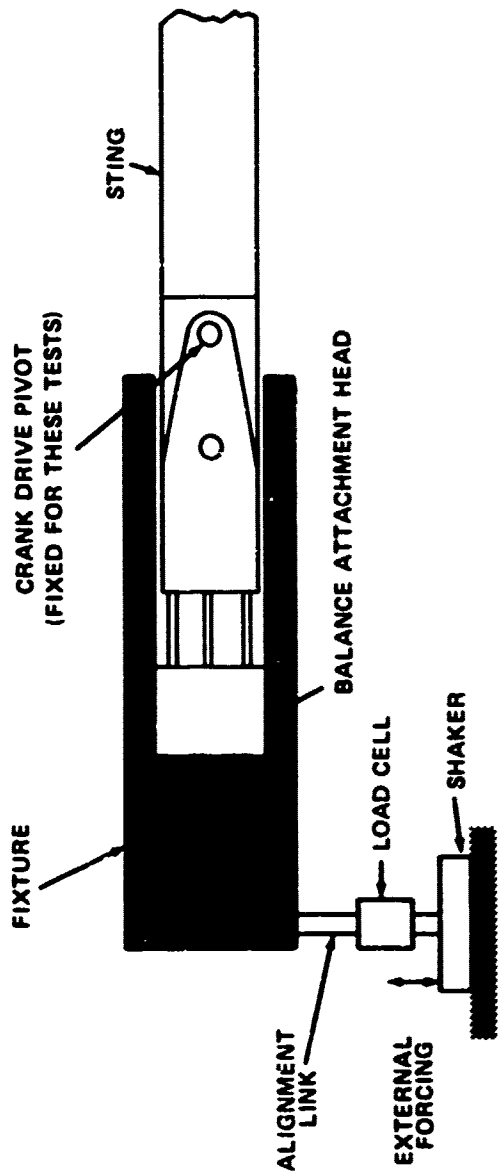

FIG. 14 SCHEMATIC DIAGRAM OF BALANCE FREQUENCY RESPONSE TEST FIXTURE

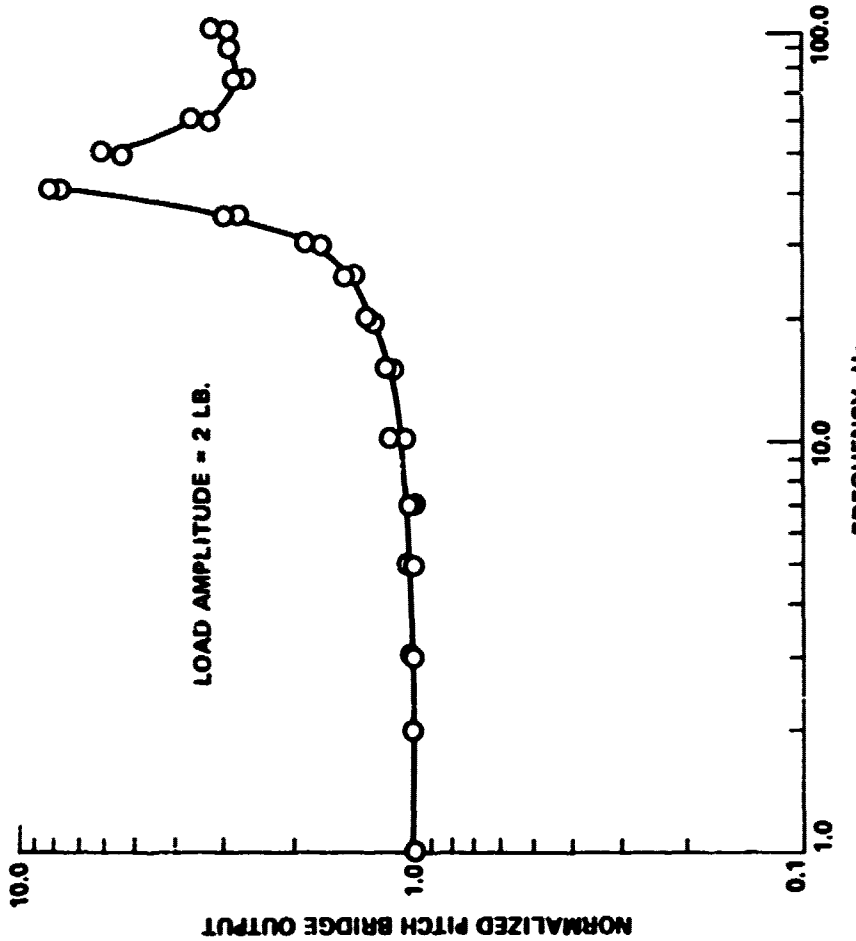

FIG. 15 TYPICAL PITCHING MOMENT BRIDGE OUTPUT AS A FUNCTION OF OSCILLATING LOAD FREQUENCY

The basic data-reduction analysis for forced-oscillation systems has been described and is not repeated here. In principle, if measurements are made of the applied moment amplitude, M_o, the angular displacement amplitude, α_o, the phase angle, ψ, between the moment and displacement signals, and the frequency of oscillation, ω, then the total system damping, C, can be computed from the relation (equation (89))

$$C = \frac{M_o \sin\psi}{\omega \alpha_o} \qquad (123)$$

When ω is approximately equal to the undamped natural frequency of the system, the phase difference ψ becomes approximately 90 degrees. At this frequency, the applied moment necessary to sustain the motion is near a minimum value. The required moment is actually a minimum at the damped natural frequency, which is slightly less than the undamped natural frequency; however, the difference between the two is negligible for lightly damped systems. Wind-off tare measurements were made under near-vacuum conditions prior to each run to assess the structural damping influence. These measurements were obtained at the wind-off resonant frequency, which was typically only one or two hertz less than the wind-on value, due to the large deflec n spring stiffness relative to the aerodynamic stiffness.

THE WIND TUNNEL TESTS

Tests were conducted in the wind tunnel facilities of the Naval Surface Weapons Center.

The Hypervelocity Research Tunnel (8A) operates (Mach 18) at temperatures up to 2400 Kelvin in the supply pressure range from 300 to 700 atmospheres. The tunnel utilizes high-pressure stored nitrogen as the working gas. The gas is heated by a forced-convection, electrical resistance-type graphite heater. Under maximum operating conditions, this heater delivers power to the gas at a rate of 1600 kilowatts.

The facility provides a maximum Reynolds number of 2×10^5 per meter, which represents altitude simulation at 36,000 meters. The average steady-state operating time at any supply condition is approximately three minutes.

The facility is supplied with a test model support mechanism that provides pitch and roll motions and readouts. Also, instrumentation and data processing equipment is available for force, pressure, temperature, and dynamic stability testing.

Nozzle flow studies; namely, Pitot pressure surveys, have been made at supply pressures of 400 and 600 atmospheres. Results of these studies indicate that the uniform flow test core is 18 to 20 centimeters in diameter. The centerline Pitot variation over a 71-centimeter axial length is approximately 3 percent. This corresponds to a Mach number gradient dM/dX of about 0.5×10^{-3}/centimeter.

For further information regarding the Mach 18 Hypervelocity Research Tunnel, see NOLTR 74-158, Ref. 10.[10]

The model was injected into the Mach 18 flow field at sting angle-of-attack of 0°, 5° and 10°, disturbed to an initial angle-of-attack and permitted to freely oscillate. The subsequent induced strain gage signals were stored on magnetic tape and converted to digital values.

The least squares-differential correction technique was then used to extract the stability parameters from the oscillatory motion.

The fitting model used was

$$\alpha = Ke^{\lambda t}\cos(\omega t + \phi) + \alpha_T \tag{124}$$

The stability coefficients determined were Cmq, the damping moment coefficient, C_m, the restoring moment coefficient, and C_{m_α} the slope of the restoring moment coefficient with angle-of-attack.

The damping moment coefficient was determined as:

$$C_{mq} = \frac{2V\lambda}{qsd}\left[2\lambda - \lambda_o \omega/\omega_o\right] \tag{125}$$

The pitching moment was determined as:

$$C_M = \frac{K\alpha_T}{qsd} \tag{126}$$

The slope of the pitching moment coefficient was determined as:

$$C_{M_\alpha} = -\frac{I}{qsd}\left[\omega^2 - \omega_o^2\right] \tag{127}$$

---

[10] Cornett, R. H. Keel, A. G., "NOL Mach 18 Hypervelocity Research Tunnel," Naval Ordnance Laboratory Technical Report 74-158, August 1974

where the assumption has been made that δ and δ_o are small compared to $4\pi^2$, see equation (60).

Results from a pitch damping investigation conducted in Supersonic Tunnel No. 2 and the Hypersonic Tunnel (8) of the Naval Surface Weapons Center, White Oak Laboratory are also presented to provide a Mach number, Reynolds number variation. The R_m/R_n = .37, 10° cone was run at a Mach number of 5 at a free stream Reynolds number of 9 x 10^6 per foot. For a discussion of the operating conditions of Supersonic Tunnel No. 2, see Reference 11.[11] Tests were also carried out in the Hypersonic Tunnel (8) at a variety of stagnation pressure conditions. For a discussion of the operating conditions of the Hypersonic Tunnel (8), see Reference 12.[12] The forced oscillation technique was also used for the hypersonic tests. The force oscillation technique was used to obtain in-plane and out-of-plane damping derivatives.

A Mach 18 free oscillation data point was also obtained in the Hypervelocity Research Tunnel for a seven percent blunt configuration.

WIND-TUNNEL RESULTS

The primary objective of the test program was to determine the aerodynamic stability coefficients for a ten degree cone as a function of bluntness and angle-of-attack under the imposed testing conditions, and to examine the repeatability of these coefficients with angle-of-attack. The results thus obtained are compared with static test results as well as results from other facilities for the purpose of evaluating the data.

Analysis of 1-D System

The free oscillation system possesses sufficient sensitivity to provide dynamic stability measurements at the Hypervelocity Research Tunnel's operating conditions. The reduceable damped oscillations thus obtained had an average mean amplitude of oscillation of approximately two degrees about a trim angle-of-attack. Sting angle-of-attack of 0°, 5°, and 10° were used throughout the testing program. The flexure pivot with the smaller torsional stiffness was selected for a majority of wind tunnel runs in order to achieve a larger amplitude of oscillation. Use of this flexure, however, resulted in large trim angles for the higher sting angles-of-attack. The flexure with the higher

---

[11] "Aero and Hydroballistics Research Facilities," Naval Ordnance Laboratory Report 1264, July 1967

[12] Geineder, F., Schlesinger, M. I., Baum, G., Cornett, R., "The U. S. Naval Ordnance Laboratory Hypersonic Tunnel," NOLTR 67-27, April 1967

torsional stiffness provided much better performance in that very small trim angles developed. It is concluded that preliminary estimates of pitching moment should be made prior to flexure selection and that these values should then be used to determine the trim angle and therefore the flexure which is most compatible with the test requirements.

No frequency effect was found to be present. The system was found to produce highly repeatable data yielding a maximum deviation of 3 percent for pitching moment coefficient and 8 percent for damping moment coefficient.

Data Reduction

The techniques previously described were used to fit the aeroballistic theory to the 1-D oscillation obtained from the wind tunnel tests.

The free-oscillation data was digitized and fit each record consisting of approximately 6000 data points. The average percent error of fit of the theory to the data indicated that the damped sinusoidal equation, Equation (121), represented the recorded wind tunnel motions to within an accuracy of 2.5 percent. A representative plot of the 1-D wind tunnel motion is presented in Figure 16.

Stability Coefficients

Representative plots of pitching moment coefficient, as determined using the free oscillation technique, versus angle-of-attack are given in Figures 17-19. These data are compared to some very accurate and precise force and moment data[13] taken for the same model in the Hypervelocity Research Tunnel. The results of the force and moment test have been carefully analyzed and numerous comparisons have been made with other experimental and analytical results. Excellent agreement is noted between the static and dynamic results over the bluntness and angle-of-attack range considered. Increase in angle-of-attack yields an increase in pitching moment. As the bluntness is increased the pitching moment is seen to increase over the range of bluntness considered.

---

[13] Keel, A., "A Note on the Viscous Effects on Center-of-Pressure Location for Sharp and Blunted Cones," Submitted to Journal of Spacecraft and Rockets, April 1975

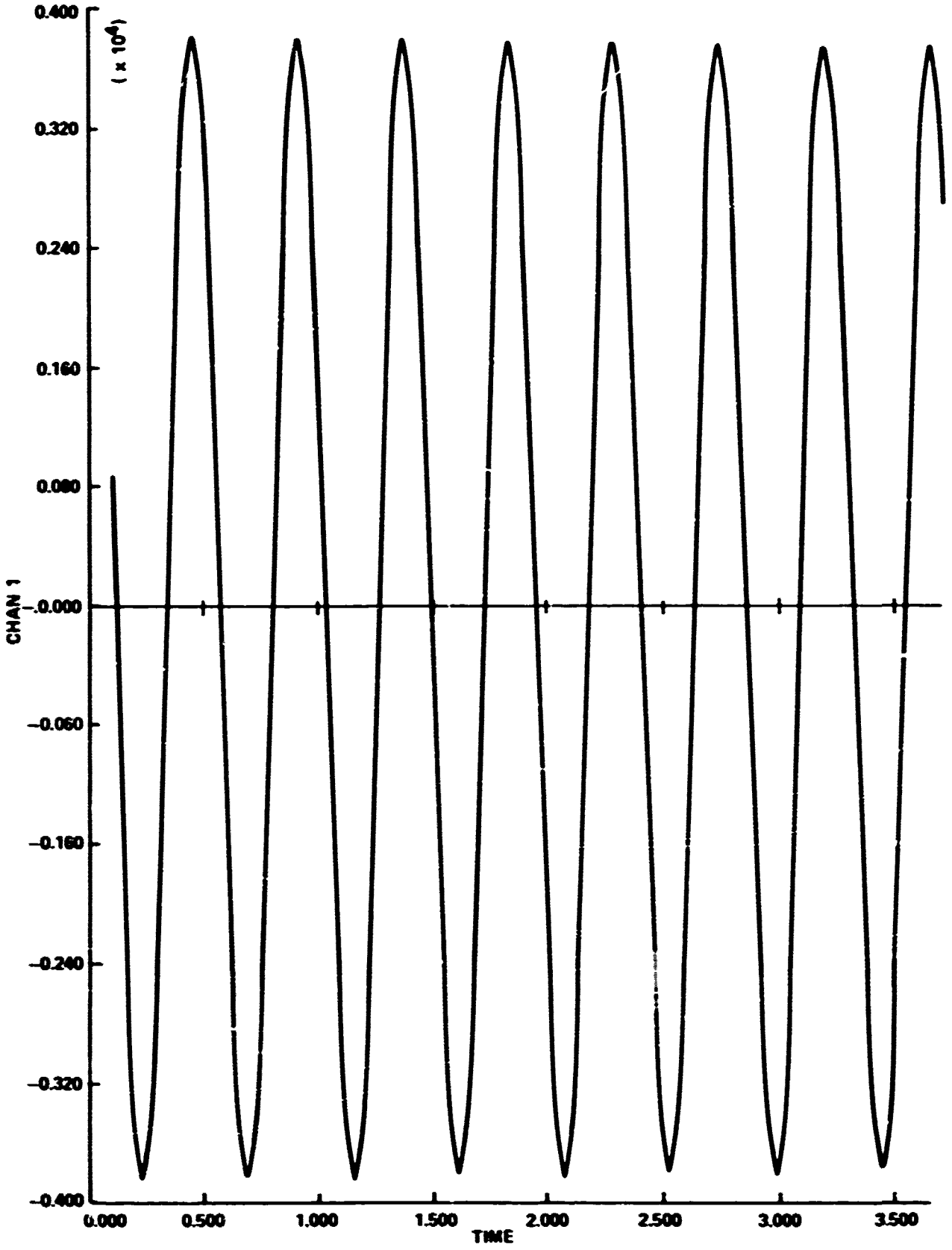

FIG. 16 3-D WIND TUNNEL MOTIONS

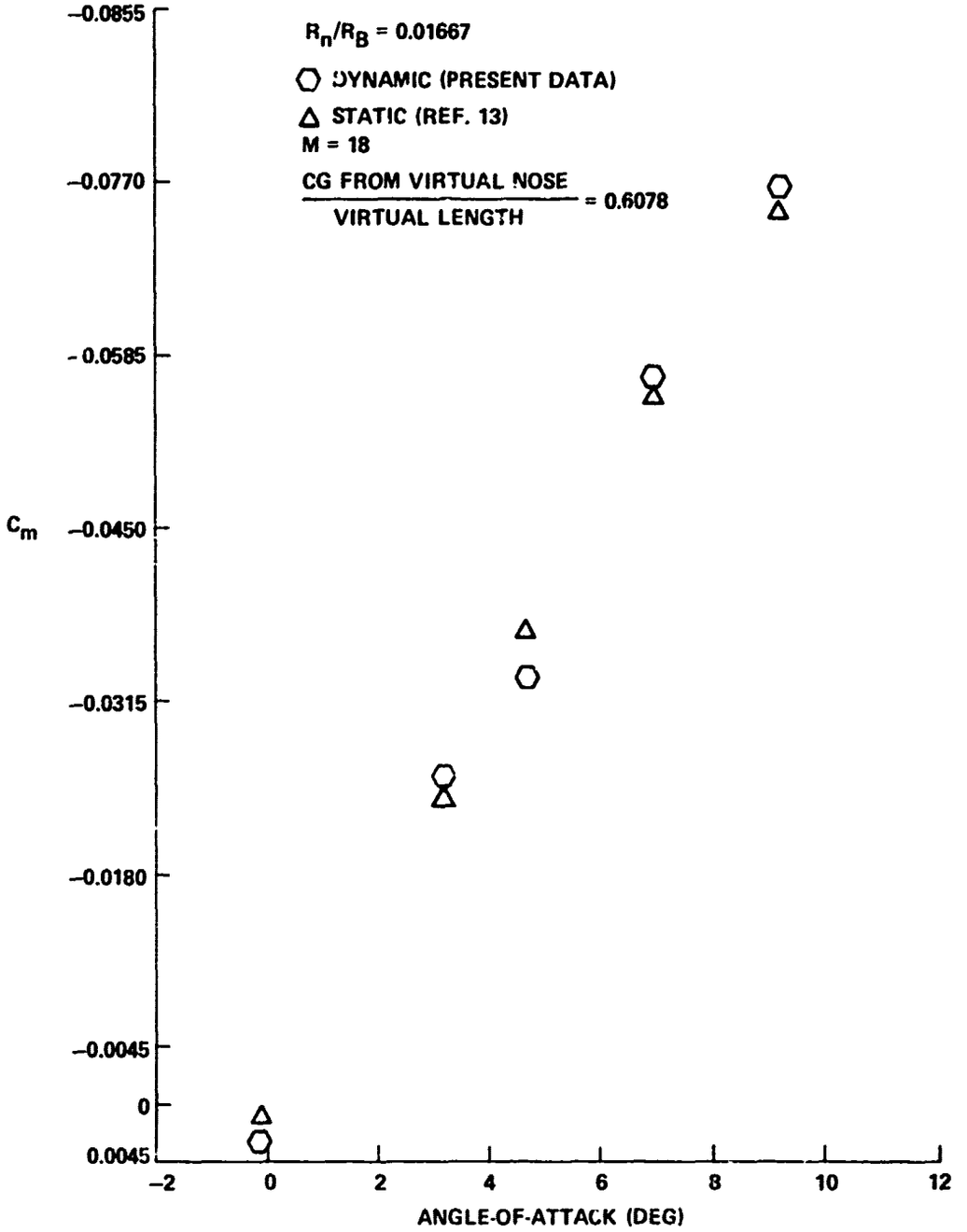

FIG. 17 PITCHING MOMENT COEFFICIENT VS ANGLE-OF-ATTACK

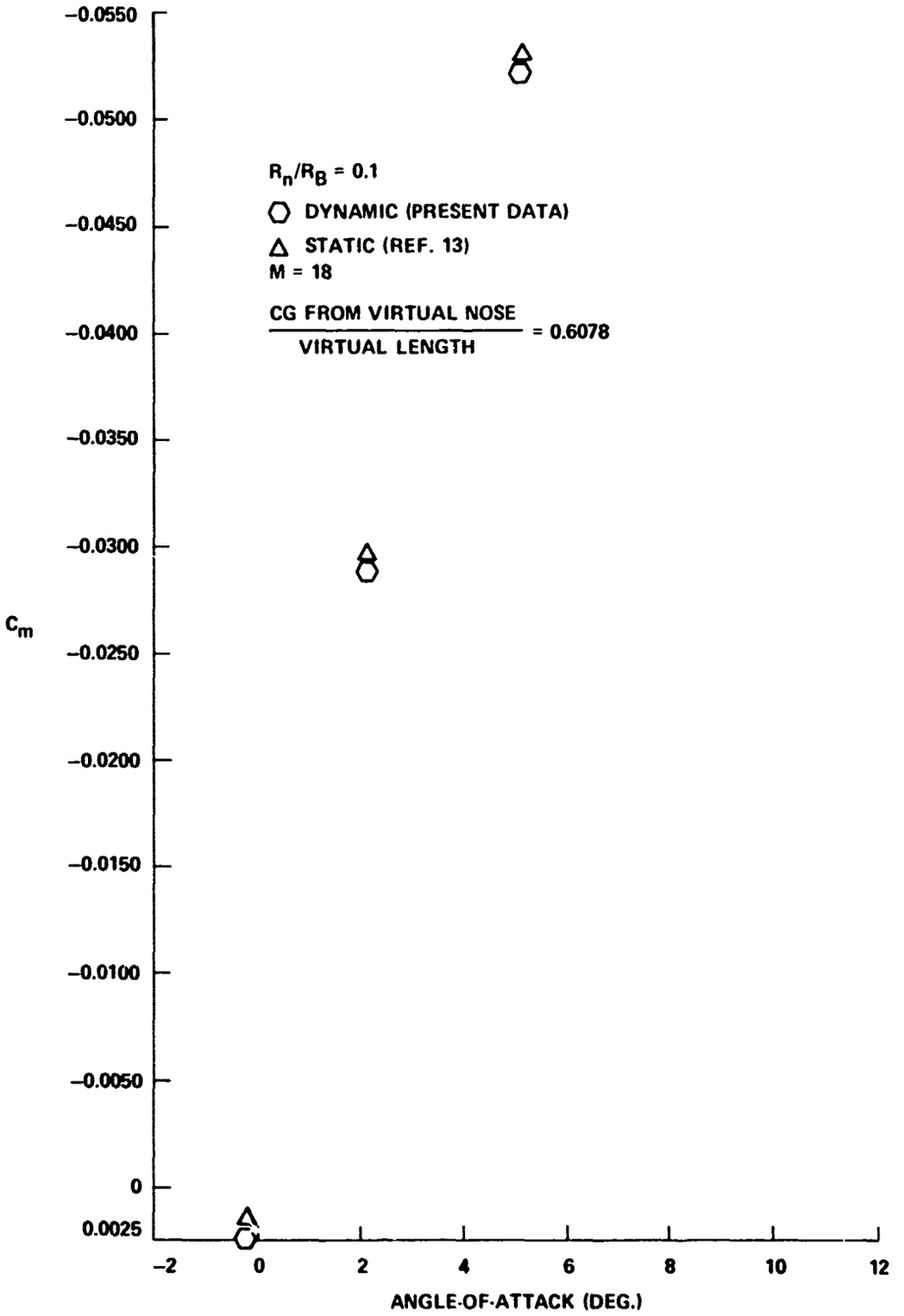

FIG. 18 PITCHING MOMENT COEFFICIENT VS ANGLE-OF-ATTACK

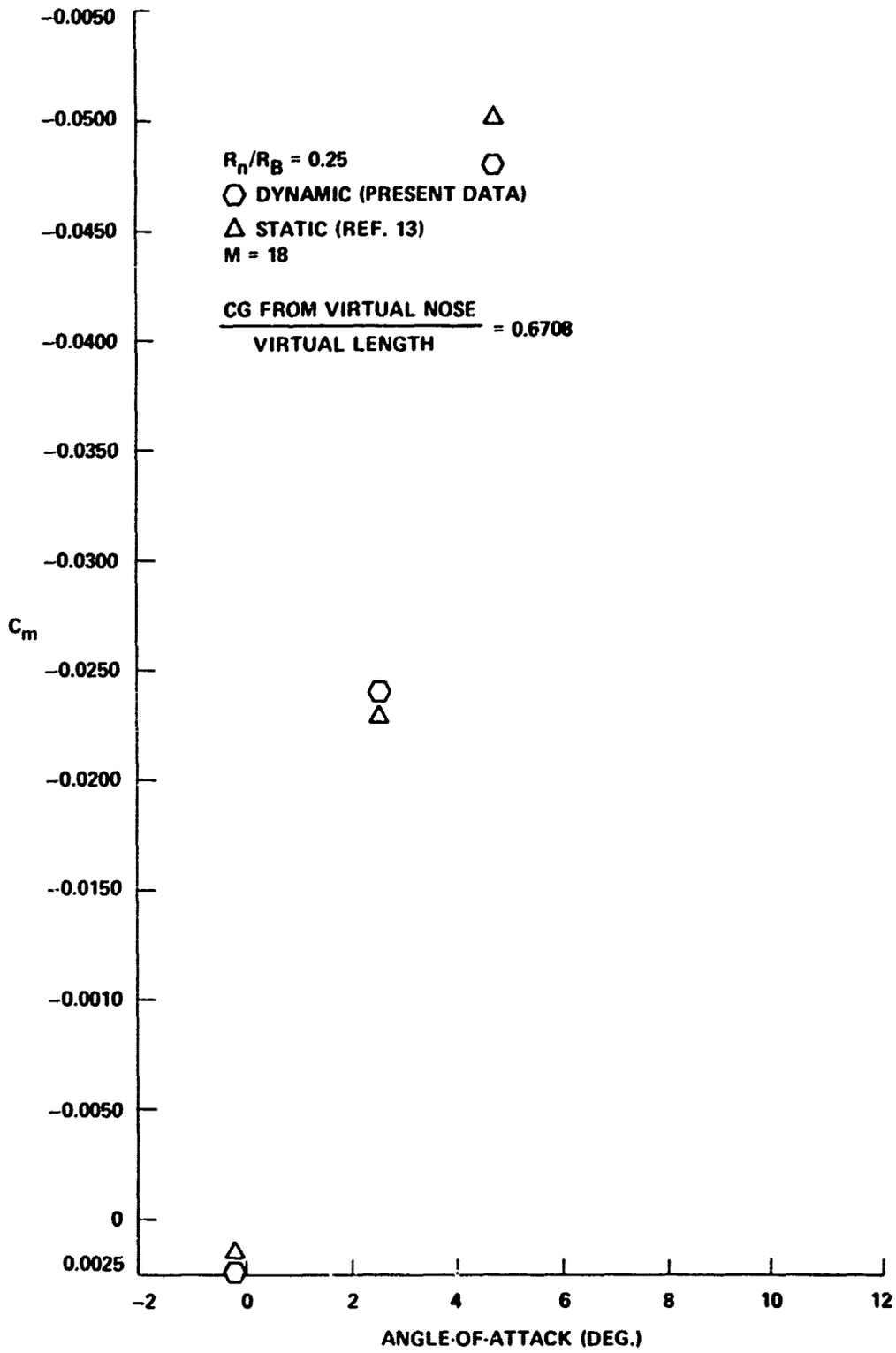

FIG. 19 PITCHING MOMENT COEFFICIENT VS ANGLE-OF-ATTACK

In order to further evaluate the free-oscillation system comparison of Mach 18 free oscillation results were made with free oscillation results obtained in the Aerospace Research Laboratory Mach 14 Facility.[14] Results typical of this comparison are given in Figures 20-25. The slope of the pitching moment curve C_{M_α} and the dynamic stability coefficient C_{M_q} are compared. The trends exhibited in the Mach 14 tests are mirrored by the Mach 18 results. The shifts noted between the Mach 14 and Mach 18 results are due to Mach number and small center of gravity location effects. The effects of bluntness on C_{M_α} and C_{M_q} are presented in Figures 26 and 27, respectively. The center of gravity location referred to the virtual nose normalized by the virtual length for the free oscillation tests had a value of 0.6078.

FORCE OSCILLATION TEST RESULTS

Tests were carried out at Mach 5 in the WOL Supersonic Tunnel (Tunnel #2) and Hypersonic Tunnel (Tunnel #8) at a variety of stagnation pressure conditions. The model used was a 10-degree cone having a nose bluntness of seven percent. The analog output signals from the strain-gage bridges were digitally sampled and recorded as a function of time, with the sampling rate being such that approximately 50 points per cycle were obtained. On-line examination of the pitching-moment and angular displacement signals displayed on a dual-trace oscilloscope provided the necessary feedback information for confirming resonant conditions. Manual motor speed control proved to be satisfactory for these tests. The phase difference between signals changed dramatically as motor speed increased through the desired resonant condition, and the moment signal minimization at resonance was quite definite. Post-test examination of the recorded signals indicated that a phase difference within a few degrees of the 90-degree resonance value was normally achieved. Checks were also made to insure that phase shifts within the instrumentation were identical for both signals of interest.

The more comprehensive testing was accomplished in the Supersonic Tunnel, with data being obtained at pitch angles of 0, 4, and 11 degrees; yaw angles of 0 and 7 degrees; and at total pressures of 30, 80, 100, 150, and 200 psia. After operation of the balance

---

[14] Walchner, O., Sawyer, F. M., "In-Plane and Out of Plane Stability Derivatives of Slender Cones at Mach 14," Aerospace Research Laboratories Report 73-0090, July 1973

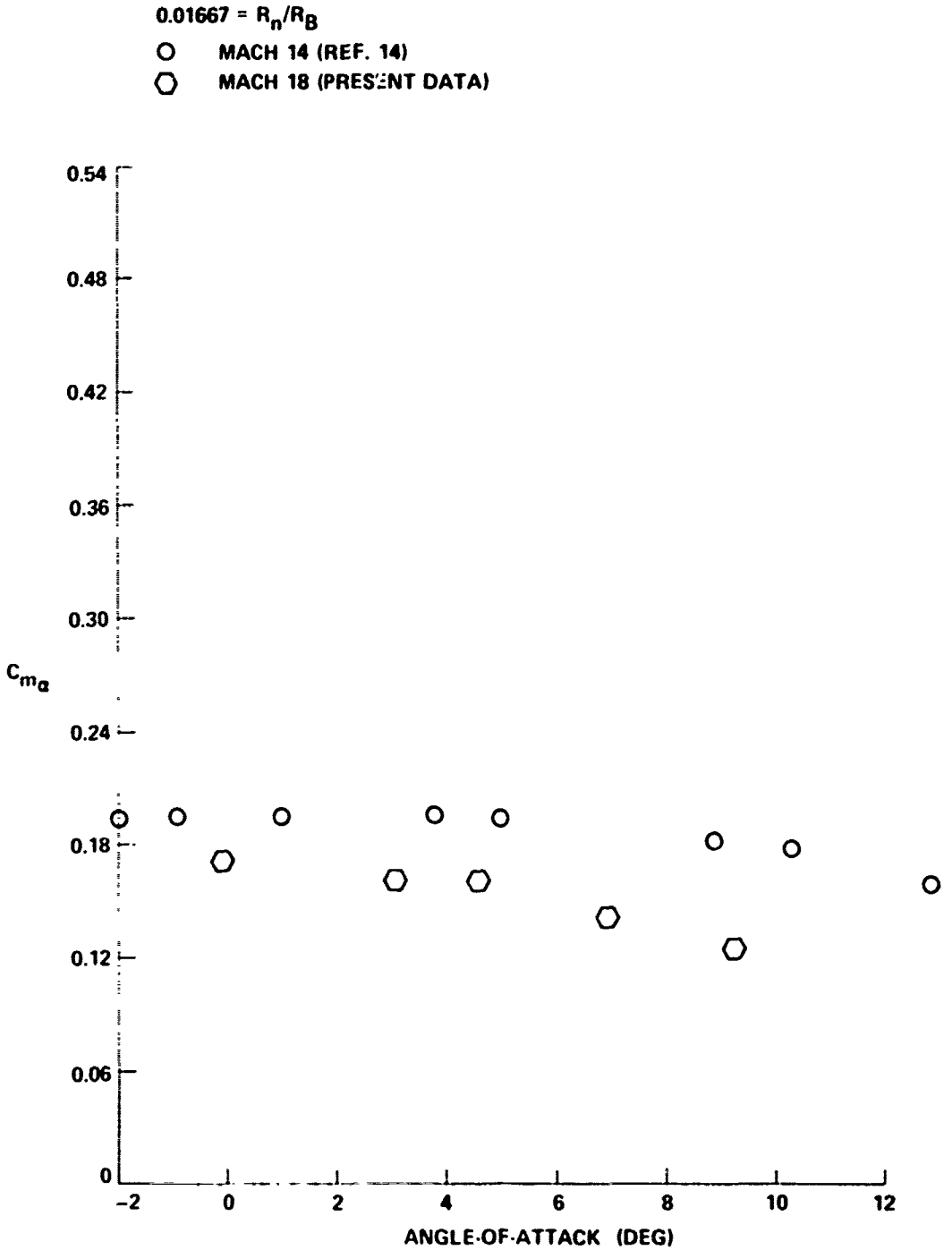

FIG.20 C_{m_α} VS ANGLE-OF-ATTACK FOR A TEN DEGREE CONE

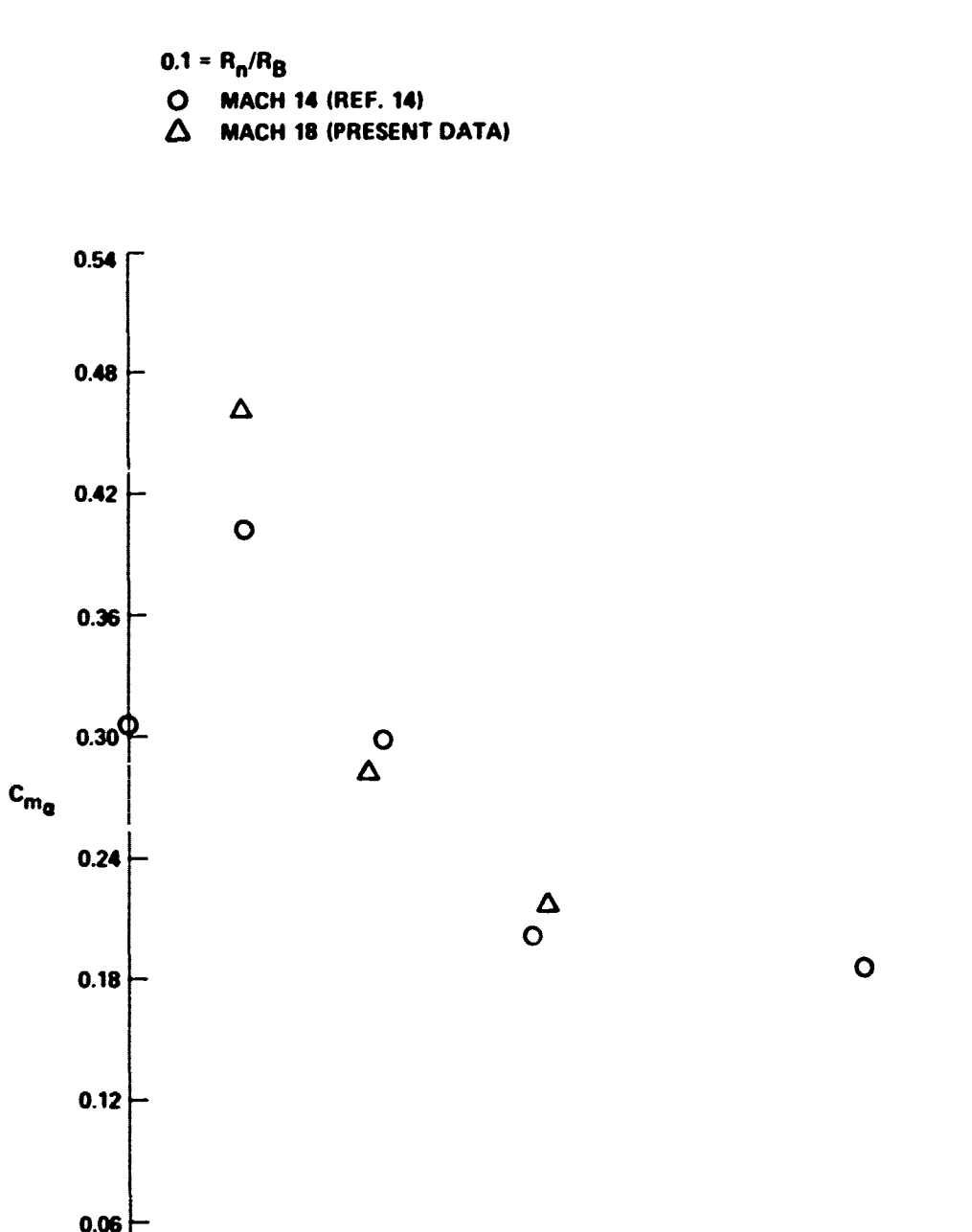

FIG. 21 C_{m_α} VS ANGLE-OF-ATTACK FOR A TEN DEGREE CONE

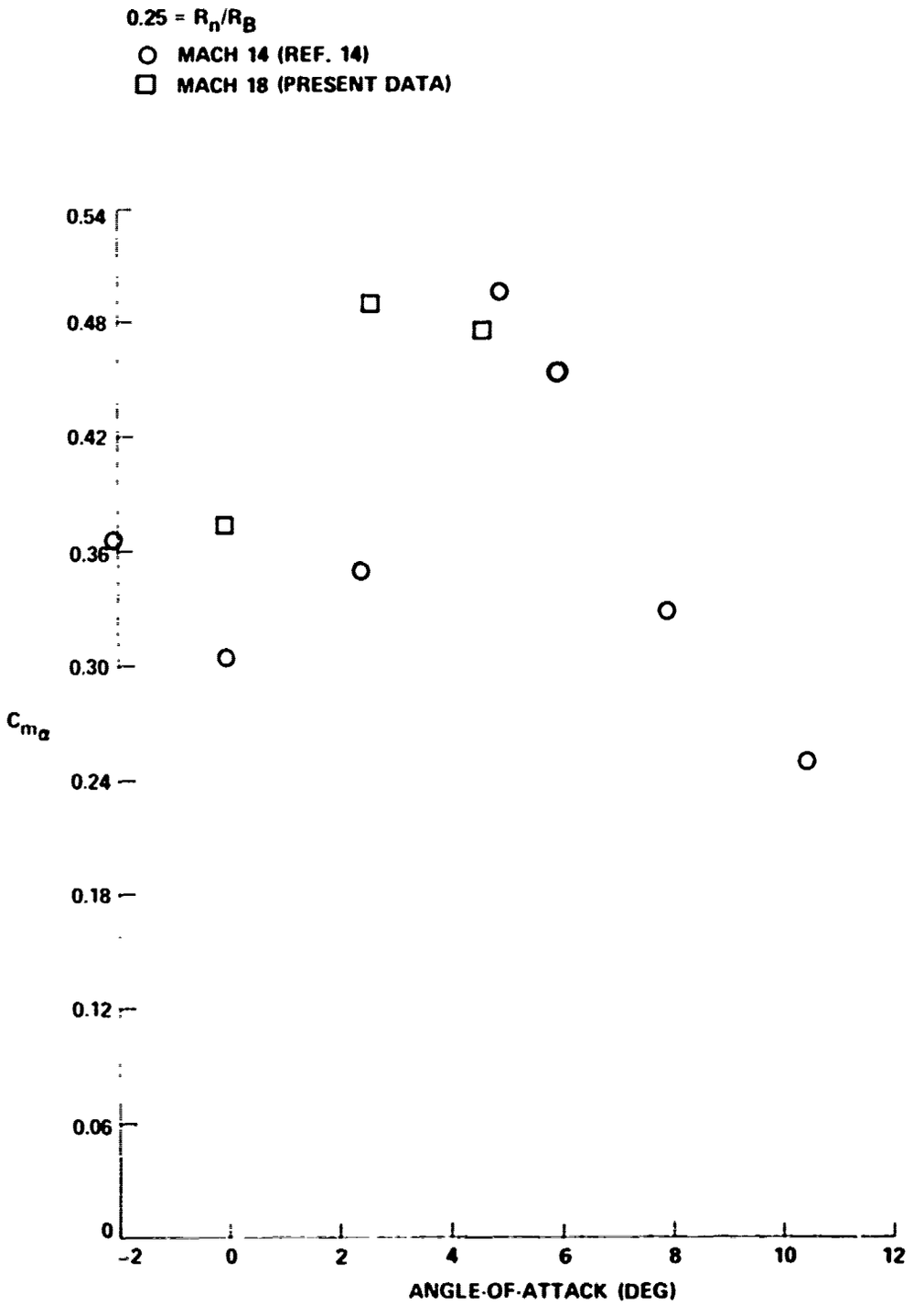

FIG. 22 C_{m_α} VS ANGLE-OF-ATTACK FOR A TEN DEGREE CONE

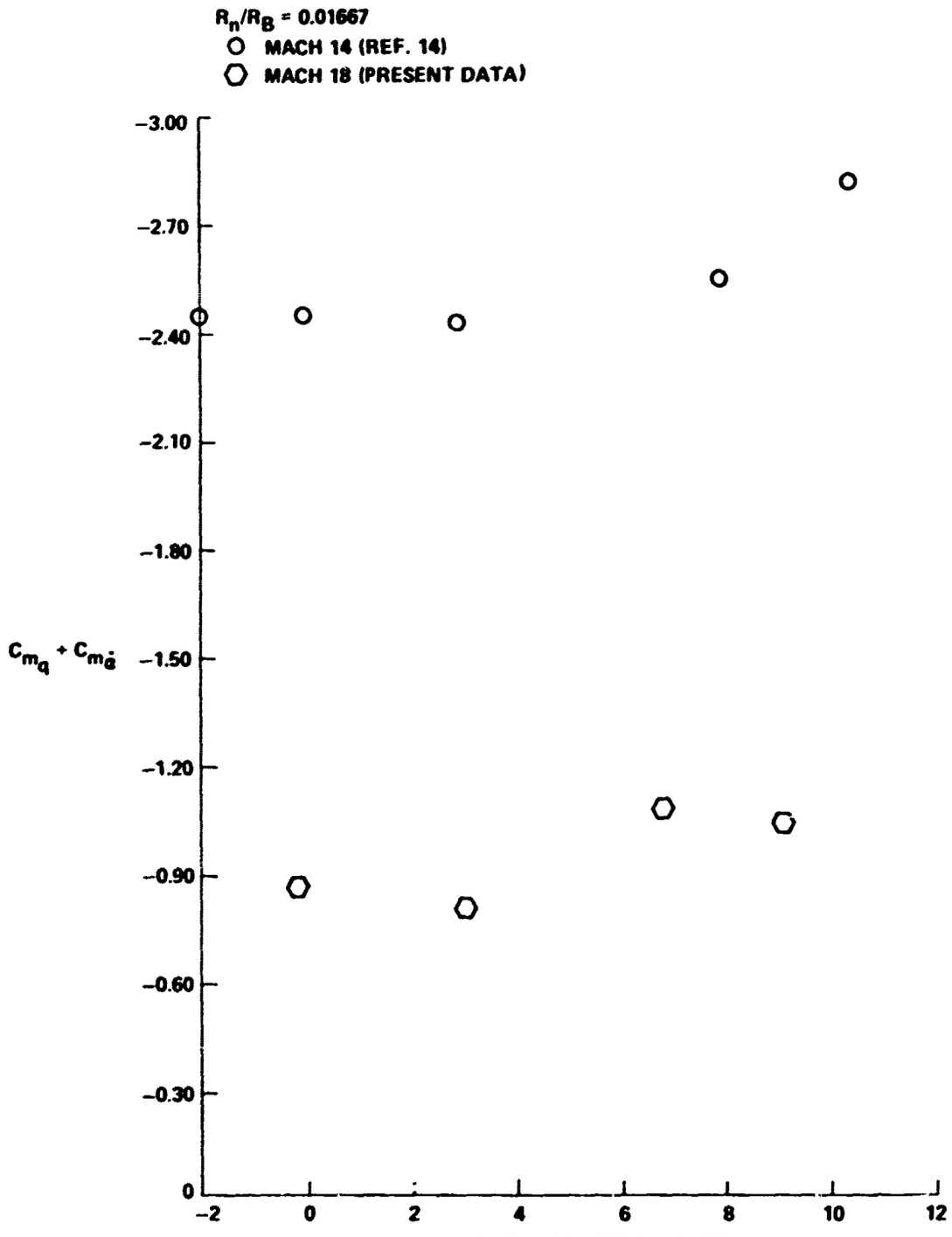

FIG.23 $C_{m_q} + C_{m_{\dot{\alpha}}}$ VS ANGLE-OF-ATTACK FOR A TEN DEGREE CONE

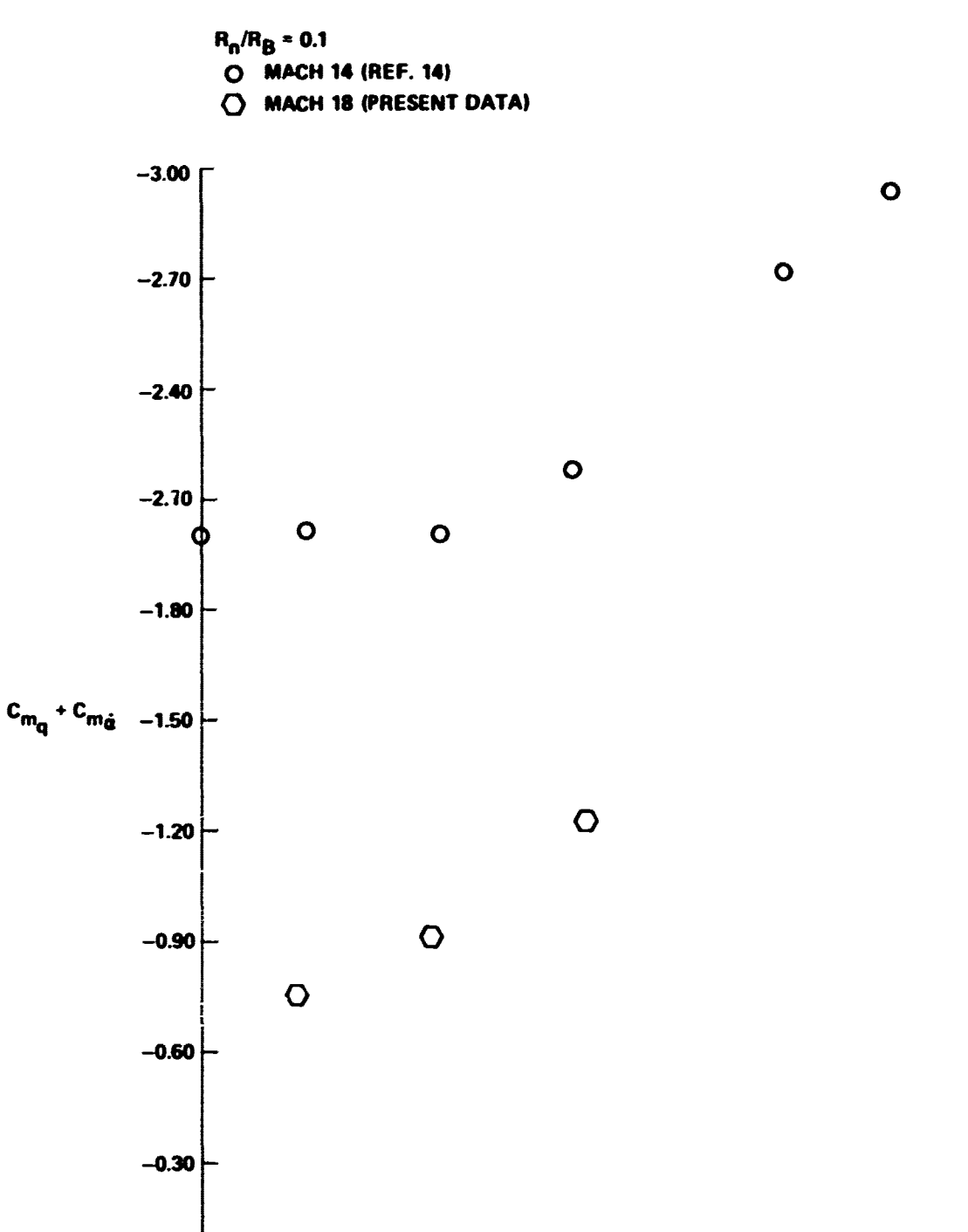

FIG. 24 $C_{m_q} + C_{m_{\dot{\alpha}}}$ VS ANGLE-OF-ATTACK FOR A TEN DEGREE CONE

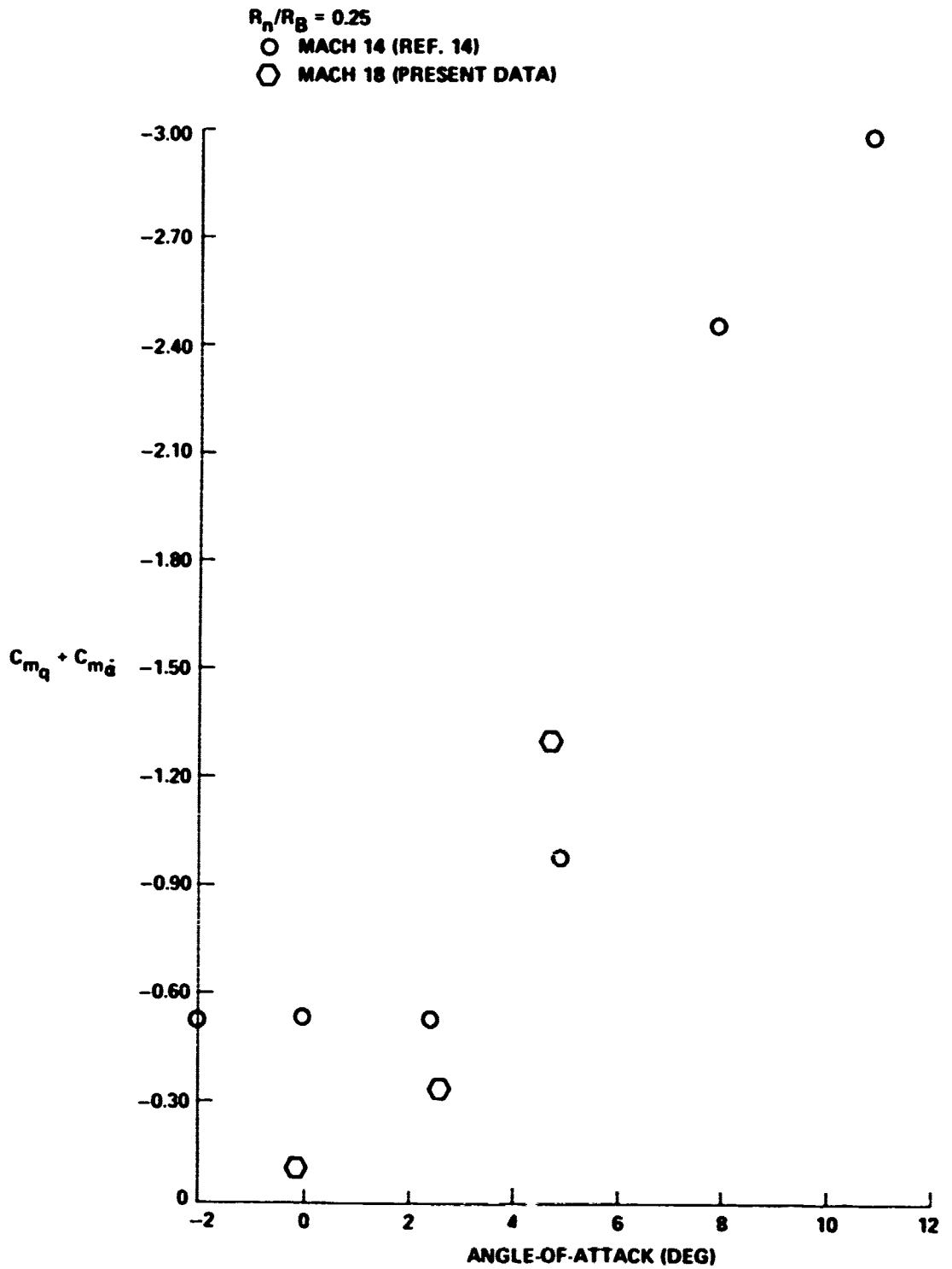

FIG. 25 $C_{m_q} + C_{m_{\dot{\alpha}}}$ VS ANGLE-OF-ATTACK FOR A TEN DEGREE CONE

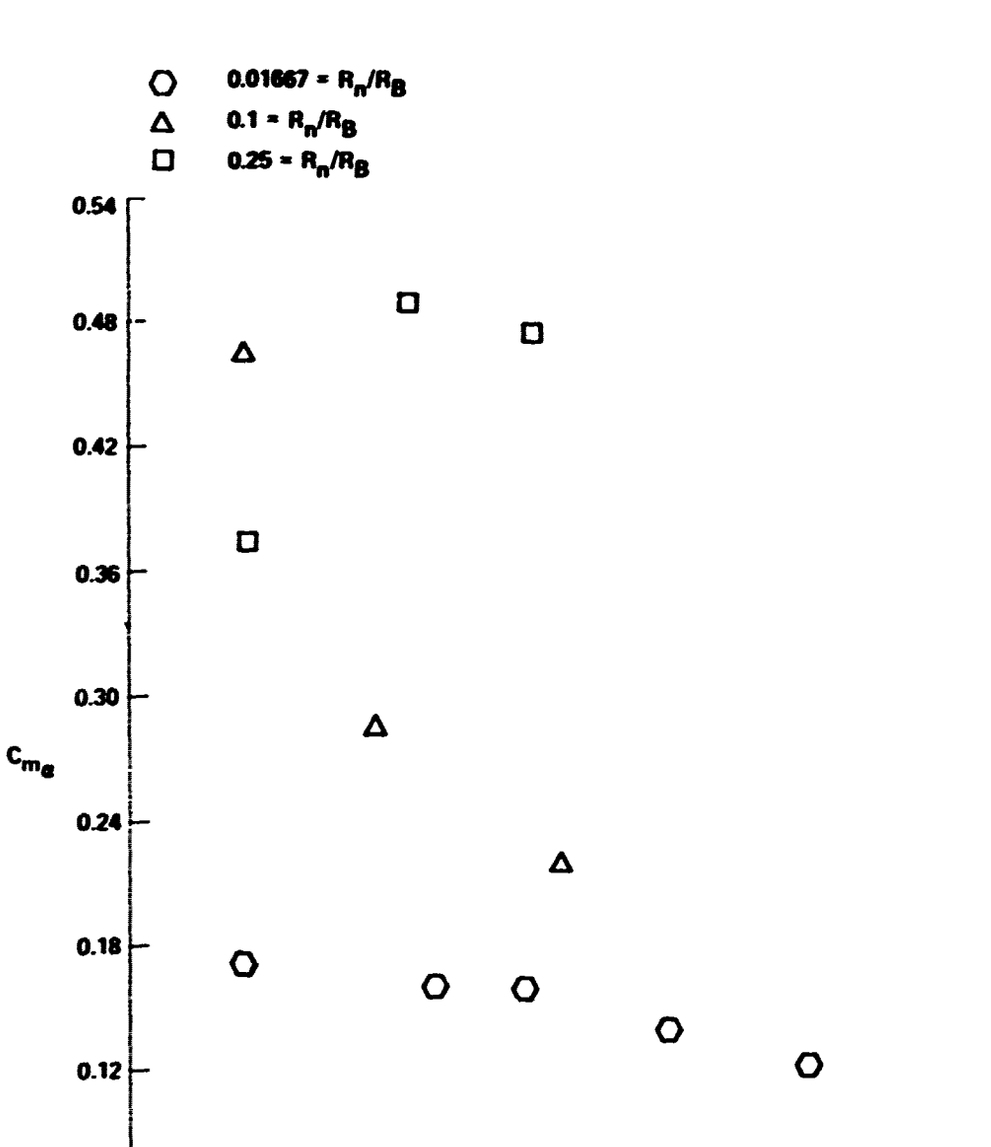

FIG. 26 C_{m_α} VS ANGLE-OF-ATTACK FOR A TEN DEGREE CONE

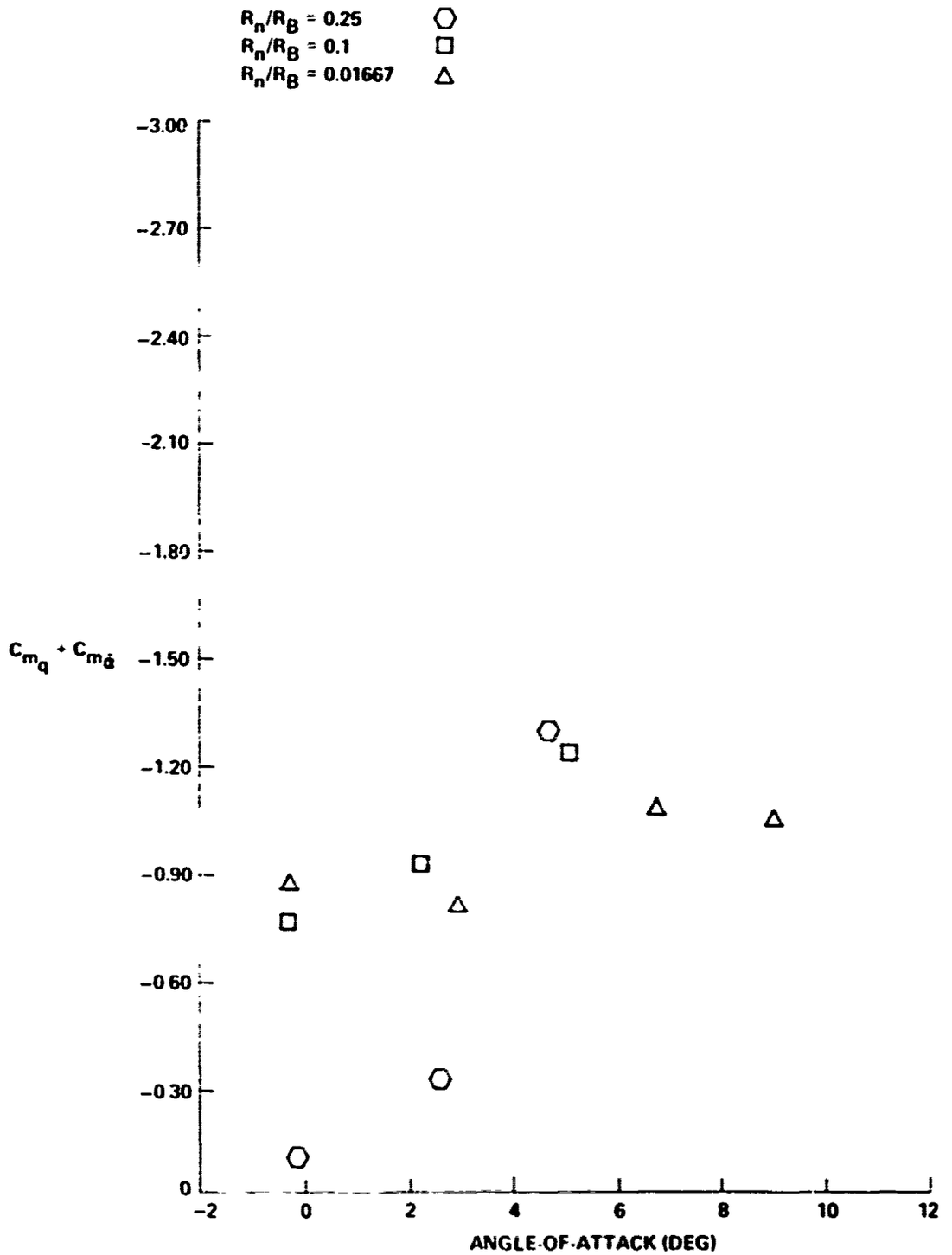

FIG. 27 $C_{m_q} + C_{m_{\dot{\alpha}}}$ VS ANGLE -OF-ATTACK FOR A TEN DEGREE CONE

and data-acquisition system was confirmed in the Supersonic Tunnel, a brief test was also conducted in the Hypersonic Tunnel at Mach 5 and at a total pressure of 370 psia to validate the balance and support system performance. Some of the results of these tests are presented in Figures 28-31 and compared with available data.

Figure 28 shows the measured damping coefficients as a function of Reynolds number and compares these results with some ballistic range data at Mach 5.7 to 7.5 (Ref. 11) and with some free-oscillation wind-tunnel data obtained at Mach 6.[15] There appears to be little Reynolds number influence on the data presented. The lowest Reynolds number at which the present data were obtained is representative of the minimum value at which the damping moment could be accurately measured at a bridge excitation voltage of four volts and with the present instrumentation setup. Balance sensitivity to lower loads can be achieved by increasing the bridge excitation (this is limited by the requirement for minimizing Joule heating of the gages and by voltage limitation of the gages themselves) and by increasing the signal gain and filtering characteristics of the data-acquisition and recording equipment.

Figure 29 presents a similar comparison of damping data as a function of Mach number. The figure includes a Mach 18 data point obtained in the WOL Hypervelocity Research Tunnel by the small-amplitude free-oscillation technique for the 7 percent blunt case. Both the Mach 5 data and Mach 18 data appear to be in reasonable agreement with available data. It should be noted that several adjustments could be made to the data to account for center-of-oscillation and nose bluntness difference but these corrections are relatively small and are not warranted for the discussion here.

The in-plane dampign data are presented in Figure 30 as a function of mean angle of attack and compared with some Mach 2 10-degree cone (R_n/R = 0.017) data. The Mach 2 data were obtained with a single-degree-of-freedom, free-oscillation balance incorporating a cross-flexure pivot.[16] The present Mach 5 data and the Mach 2 data indicate no significant angle-of-attack effects for angles less than the cone half angle. An out-of-plane damping data point obtained at an angle of attack of seven degrees with the present forced-oscillation technique ($C_{mq} + C_{m\dot{\alpha}} = -30$ was obtained) also agrees in a similar manner with the Mach 2 out-of-plane damping data of Reference 16. However, the out-of-plane data do not indicate the rather definite increase in

---

[15] Preslin, R. F., "High-Amplitude Dynamic Stability Characteristics of Blunt 10-Degree Cones," TR 32-1012, Jet Propulsion Laboratory, Pasadena, California, October 1966

[16] Stone, G. W., Clark, E. L., Jr. and Burt, G. E., "An Investigation of Nonsymmetrical Aerodynamic Damping Moments," AIAA Paper 72-29, January 1972

SYMBOL	SOURCE	M	R_n/R_B	CG, %	$\omega D/2V$
○	(PRESENT DATA)	5	0.07	67	0.004
□	JPL (WIND TUNNEL DATA, REF. 15)	6	0.0	66	0.001 TO 0.005
△	AEDC (RANGE DATA, REF. 1)	5.7 TO 7.5	0.032	65	0.001 TO 0.003

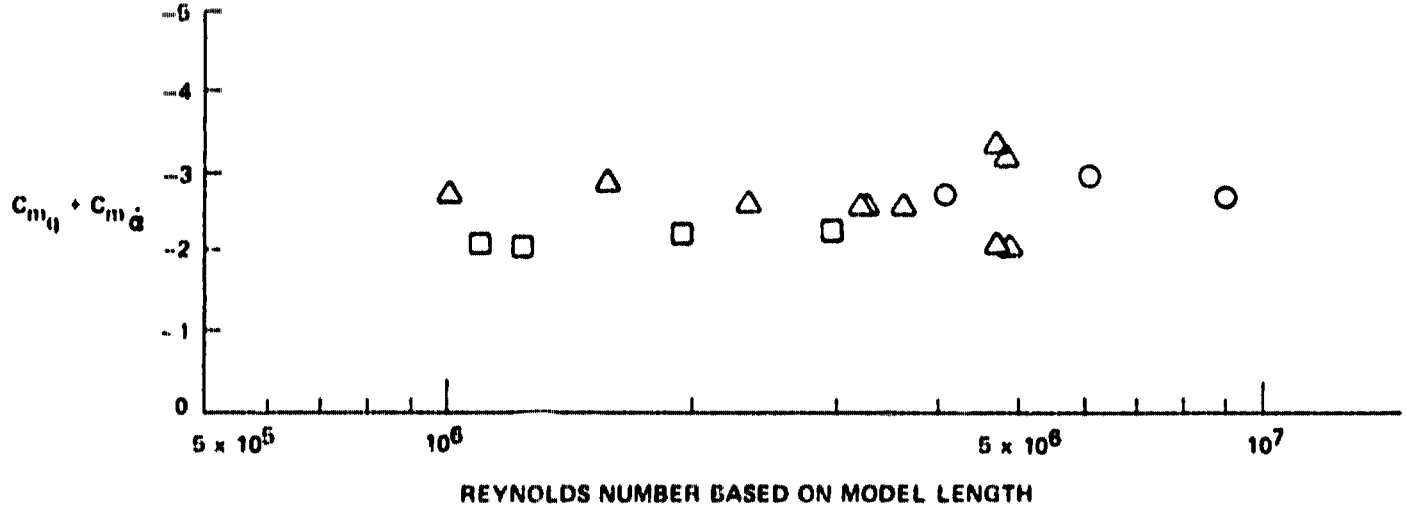

FIG. 28 DAMPING DERIVATIVE AS A FUNCTION OF REYNOLDS NUMBER AT MACH 6 FOR A 10-DEGREE CONE

SYMBOL	SOURCE	Re	R_N/R_B	CG%	$\omega D/2V$
⬡	(PRESENT DATA)	9×10^6	0.07	67	0.004
◇	(PRESENT DATA)	0.5×10^6	0.07	67	0.003
▱	JPL (WIND TUNNEL DATA, REF. 15)	$\approx 0.8 \times 10^6$	0.0	64	≈ 0.005
◇	AEDC (RANGE DATA, REF. 1)	0.4×10^6	0.032	63	0.001 TO 0.002
○△▽□◊	WIND TUNNEL DATA (SEE REF. 1)	0.2×10^6 TO 0.6×10^6	0.0 TO 0.017	55 TO 60	0.003 TO 0.015

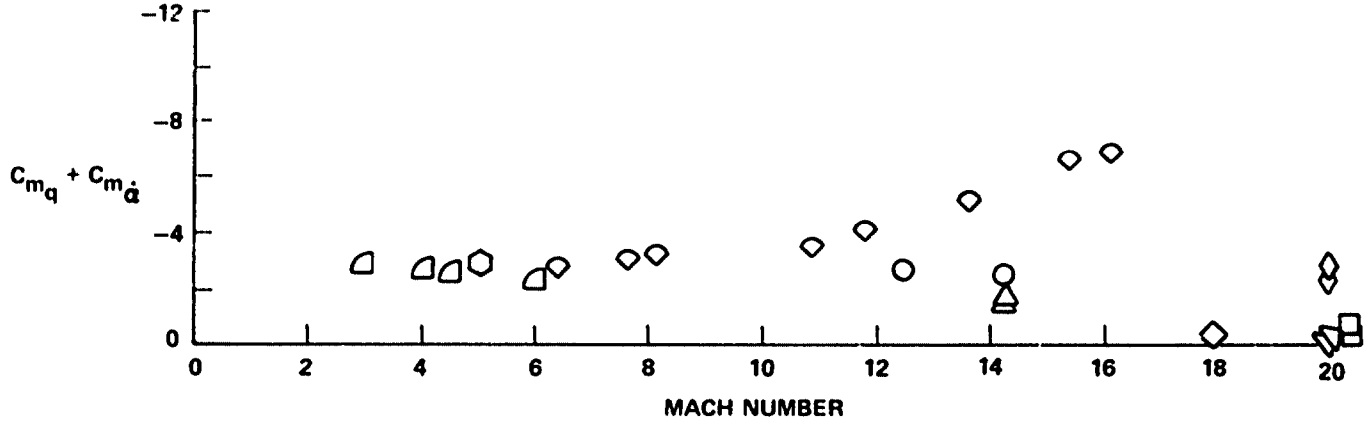

FIG. 29 DAMPING DERIVATIVE AS A FUNCTION OF MACH NUMBER FOR A 10-DEGREE CONE

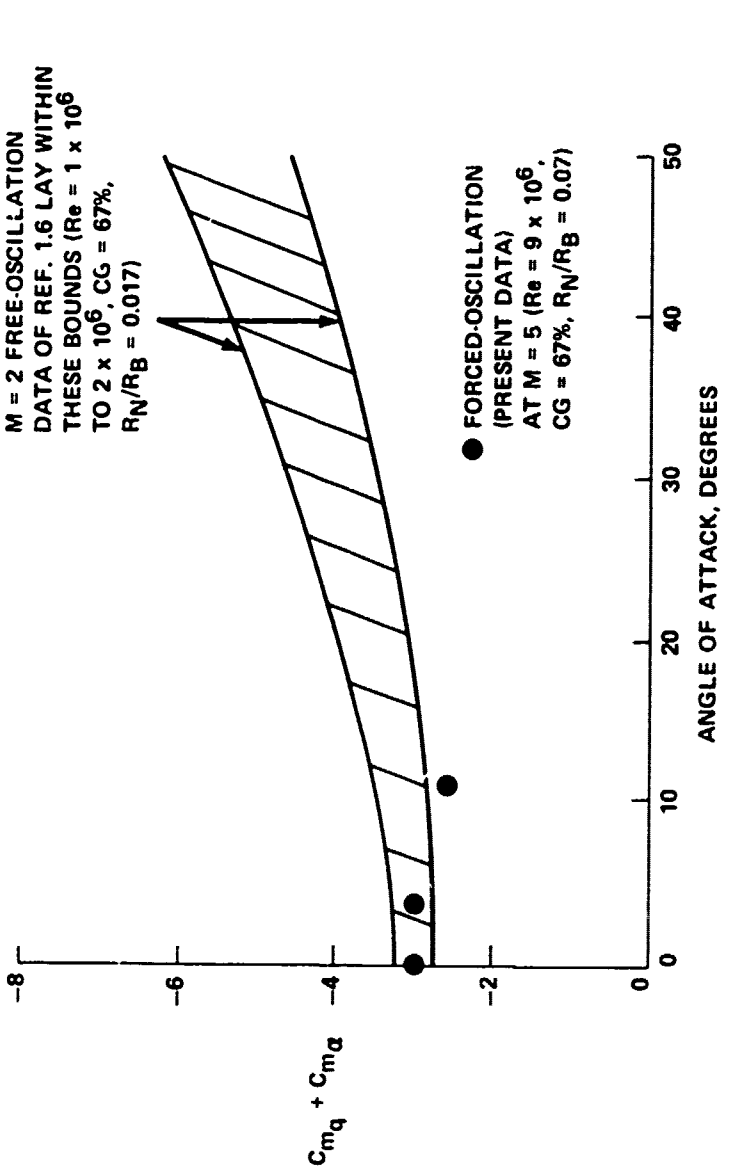

FIG. 30 IN-PLANE DAMPING DERIVATIVE AS A FUNCTION OF ANGLE OF ATTACK FOR A 10-DEGREE CONE

damping at an angle of attack near the cone half angle, but rather they indicate some decrease in damping for this configuration as angle of attack approaches 30 degrees or so.

Finally, a data point was obtained at zero mean angle of attack in the WOL Hypersonic Tunnel for the 7 percent blunt case. The results obtained were in agreement with the data obtained in the Supersonic Tunnel. The balance support system in the Hypersonic Tunnel does not permit out-of-plane damping data to be obtained with this particular balance; however, in-plane damping may be obtained at angles of attack up to 30 degrees, a limit imposed by the necessity for maintaining an adequate oil both for the motor gearing in the drive-unit housing of the balance, discussed earlier. The allowable load limits imposed by the mechanical design of the balance were not reached in any of the tests reported here, and therefore the balance possesses the capability for use at higher loads (i.e., higher total pressures) than indicated by these evaluation tests.

RANGE WIND-TUNNEL PITCH DAMPING DISCREPANCIES

Reference 1 reports an increase in dynamic stability as Mach number is increased. As a result of this range conducted investigation, it was concluded that the measurements made suggest that the damping derivatives at higher Mach numbers may have some dependence on the type of motion pattern experienced by the model. As previously seen, in comparing the data of Reference 1 with comparable wind tunnel data, the wind tunnel determined values indicate a decrease in dynamic stability with Mach number, which is not in agreement with the results of the range study. No Reynolds number variation can be seen to contribute as was shown in Figure 28. Reference 1 also concludes that the reported discrepancies may be due to model support interference. During the present investigation, no conclusive evidence of this type of interference could be determined. The high repeatability of the data and the excellent agreement noted with the static test results and results from other facilities tend to de-emphasize this conclusion. It is felt, however, that this discrepancy may be explained by a difference between the in plane and out of plane dynamic stability coefficients. Such results were first reported for angles-of-attack greater than the cone half angle (Ref. 16).

Tabok and Schiff[17] suggested a theoretical moment formulation for nonplanar vehicle motion. This formulation was nonlinear with respect to angular displacement and linear with angular rates.

---

[17]Tobak, M., Schiff, L., "A Nonlinear Aerodynamic Moment Formulation and Its Implication for Dynamic Stability Testing," NASA Ames Research Center, AIAA Paper 71-275, 1971

It was concluded that yaw damping at angle-of-attack must be different from pitch damping if the pitch moment is a nonlinear function of angle-of-attack. It has been shown that slightly blunted cones have highly nonlinear aerodynamics at small angles-of-attack, which are only a fraction of the cone half angle (References 14 and 18)[18] and subsequent analysis followed.[19]

Two-degree-of-freedom tests have also been conducted[20] to investigate the in-plane, out-of-plane defference. It was found that a transverse product of inertia has a very strong coupling effect in the case of nonplanar motion. In the case of planar motion linear aerodynamics were experienced. In the case of nonplanar motion an aerodynamic accleration coupling derivative was extracted which had the same effect as an inertial coupling by-product of inertia.[21]

Such damping asymmetry tends to invalidate the use of the tri-cyclic theory to correctly represent the free flight motion of blunted sphere cones. Out-of-plane damping is then present in the range test and is not present in the wind tests.

---

[18] Clay, J. T. and Walchner, O., "Nose Bluntness Effects on The Stability Derivatives of Slender Cones," Transactions of the Second Technical Workshop on Dynamic Stability Testing, AEDC and ARO, Inc., Vol. 1, Paper 8, 1965

[19] Murphy, C., "Limit Motions of a Slightly Asymmetric Re-entry Vehicle Acted on by Cubic Damping Moments," U. S. Army Ballisitcs Research Lab., Aberdeen Proving Grounds, Maryland, AIAA Paper 74-870, 1974

[20] Yelmgren, K. E., Sawyer, F. M., Walchner, O., "Stability Derivatives of a 10° Cone Existing Planar and Non-Planar Motion at Mach 14," Aerospace Research Laboratories, Wright-Patterson AFB, Ohio, ARL 74-0112, August 1974

[21] Walchner, O., "Research on Hypersonic Stability Problems," Aerospace Research Lab. Report 74-140

If the range data were fit without allowing for this in-plane, out-of-plane difference an error will be introduced which could lead to the over prediction of total damping. As the Mach number is increased the initial angular disturbance of the range model would increase and thus the resulting oscillations and the over prediction of total dynamic stability coefficient.

The reported in-plane, out-of-plane damping difference should be further investigated. A corrected equation of motion should be determined and simulation conducted to determine the overall effect of such coefficient asymmetry. In the meantime, care should be taken in comparing results determined from methods where in-plane, out-of-plane damping is present and methods where only in-plane damping is present until the source for the disagreement is well understood.

SUMMARY

The damping in pitch characteristics of a ten degree cone have been investigated. Numerous single-degree-of-freedom wind tunnel experiments have been conducted in order to obtain the variation of damping coefficient with bluntness, Mach number, Reynolds number and angle-of-attack. The results of the present investigation have been compared with results from other facilities and have been found to be in good agreement. Data on the ten degree Supersonic Tunnel Association cone was also obtained at Mach 18. Damping data on this configuration at Mach 18 was not previously available. A discrepancy was noted with damping data variation with Mach number as obtained from a ballistic range experiment. An explanation of this discrepancy, based on in-plane, out-of-plane damping difference, has been offered. A detailed explanation of the theory, data reduction technique and experimental methods has also been presented in order to document the dynamic testing capabilities of the Naval Surface Weapons Center, White Oak Laboratory.